Analytical solutions for strong field-driven atomic and molecular one- and two-electron continua and applications to strong-field problems

Olga Smirnova,[1] Michael Spanner,[2] and Misha Ivanov[1]
[1]*National Research Council of Canada, Ottawa, Ontario K1A 0R6, Canada*
[2]*Chemical Physics Theory Group, Department of Chemistry, and Center for Quantum Information and Quantum Control, University of Toronto, Toronto M5S 3H6, Canada*
(Received 13 November 2007; published 11 March 2008)

We develop the eikonal-Volkov approximation (EVA) to describe atomic and molecular strong-field dynamics. The main component of this approach is the approximate solution for the continuum states of one and two electrons in the presence of a long-range ionic potential and a strong laser field. These solutions include the laser field fully, the ionic potential, and the electron-electron interaction in the eikonal approximation, and describe the nonperturbative coupling between these interactions. Comparison with numerically evaluated continuum electron wave functions demonstrates quantitative accuracy of the approximate solutions. Their long-time limit yields the quasienergy (Floquet) states of the continuum electron. We also show how to extend the applicability of these solutions to deal with the singularities of the ionic potential, where straightforward eikonal approximation breaks down. The large-angle scattering (hard collision) is incorporated in the EVA formalism using an expansion in the number of hard collisions. Finally, we describe how the EVA formalism can be used to obtain simple analytical expressions for various strong-field problems.

DOI: 10.1103/PhysRevA.77.033407 PACS number(s): 33.80.Rv, 42.50.Hz, 33.80.Wz

Imaging the dynamics of electrons in atoms and molecules is one of the key goals and most challenging problems in ultrafast physics. Intense laser pulses open new avenues for addressing this problem. Essentially all strong field phenomena, e.g., above threshold ionization (ATI) [1,2], high-order harmonic generation (HHG) [3], and nonsequential double ionization (NSDI) [4] can be used for imaging bound and continuum electron dynamics in atoms and molecules [5–12]. Strong laser fields offer unique opportunities for combining attosecond temporal and sub-Å spatial resolution, but at the same time bring significant complications by inducing complex nonperturbative interactions. Information about the electron dynamics is hidden in ATI, HHG, and NSDI spectra and the quality of its retrieval depends on the quantitative accuracy of the theoretical approaches used to describe and analyze these spectra.

The majority of strong field effects can be qualitatively understood within the strong field approximation (SFA) [13–15], which neglects the Coulomb interaction of a continuum electron with the parent ion, representing the continuum with plane wave Volkov states [16]. Even though the strong laser field may dominate the continuum dynamics, as a rule this approximation does not provide quantitative accuracy. In some cases it may also yield an incorrect qualitative picture as explored in Ref. [17].

This paper aims at keeping the universality of the SFA while including the scattering potential nonperturbatively, taking advantage of simplifications introduced into the scattering problem by the strong laser field. Approximate approaches developed so far, which go beyond the SFA by including the interaction of the continuum electron with the Coulomb potential, do not have SFA's appealing universality. Instead, they are problem-specific.

The first example is "fast" ionization resulting from the one-photon bound-continuum transitions in a hydrogen atom or a hydrogen molecular ion in the presence of a strong laser field. In this case, one can substantially simplify the problem by neglecting the coupling between the Coulomb and the laser fields in the continuum electron dynamics. This approximation uses the Coulomb-Volkov ansatz [18–22] for the continuum wave function of the strongly driven electron. Recently, this approximation has been applied to the analysis of photoelectron spectra [23,24] and high-order harmonic spectra [25] for H_2^+. As the frequency of one-photon transition decreases or the size of the molecule increases, one can no longer ignore the effects of the Coulomb-laser coupling [26] and this approximation breaks down. It is also unlikely that one could extend the Coulomb-Volkov ansatz to arbitrary scattering potentials.

The second example involves "slow" ionization by a strong infrared field. In this case the Coulomb effects can be included quasiclassically [27]. This approach uses the quasiclassical action, evaluated along the electron trajectories in the classically forbidden region, as the electron is moving under the barrier formed by the laser field and the ionic potential. Its applicability requires substantial thickness of the barrier (i.e., action large compared to $\hbar$). For small values of the Keldysh parameter [13] $\gamma \ll 1$, this approach is valid for moderate fields with strength $\mathcal{E} \ll (2I_p)^{3/2}$. Here $\gamma^2 = I_p/2U_p$, I_p is the ionization potential of the system and $U_p = \mathcal{E}^2/4\omega^2$ is the average electron oscillation energy in the laser field with frequency ω and electric field amplitude $\mathcal{E}$. (Atomic units are used throughout.) In the multi-photon limit of large $\gamma \gg 1$, this approach is only valid for low laser field frequencies $\omega \ll 2I_p$ [see Eq. (53) of Ref. [28] and Eq. (37) of Ref. [27]].

We describe an approximate approach that can be applied on equal footing to essentially all strong field problems. It is almost equally accurate for both "slow" and "fast" ionization problems [17,29]. In this approach the electron motion in the continuum is modeled by including the laser field fully and the ionic potential in the eikonal approximation (see, e.g., [30]). It is rooted in the pioneering works by Popov and

co-workers [31,32], where the eikonal approximation was first introduced into the problems of strong field ionization. This approach, which we refer to as the eikonal-Volkov approximation (EVA) inherits the key strength of SFA: Universality, physical transparency, and adaptability to the analytical analysis.

This paper describes several key results that extend our previous work on the eikonal-Volkov continuum states [17,26,29]. These continuum states were first introduced by Gersten and Mittleman [33] for the problems of electron scattering in the laser field and further generalized in Ref. [34]. See also Refs. [35–37] for similar approaches. The key results are indicated below.

(1) We present detailed derivations of both the phase and amplitude corrections to the Volkov function [16], which are applicable for arbitrary 3D scattering potentials. We demonstrate the accuracy of the phase and amplitude corrections through a comparison with numerical solutions in 1D case. The amplitude corrections improve the eikonal approximation introduced in Ref. [33] in the way similar to generalized eikonal approximation of Ref. [34]. To gauge the accuracy of the phase and amplitude corrections in 3D, we compare the exact and approximate one-photon bound-free dipole matrix elements for hydrogen atoms (Sec. VI D).

(2) We describe further approximations to the eikonal-Volkov states that simplify the analytical expressions for their phase and amplitude. We analyze the quantitative accuracy of these approximations both for the wave functions and for observables.

By construction, the eikonal-Volkov states remain in the continuum both during and after the laser pulse. Therefore, the eikonal-Volkov propagator does not include coupling to the ground state or other bound states. In other words, this propagator operates in a restricted sub-space of the complete Hilbert space of the system. We show how the so-called Adams' partitioning procedure allows one to deal with such propagators. In particular, we stress that the Adams' partitioning procedure clearly implies dressing of the initial state, as opposed to the standard strong-field S-matrix expressions where the initial state remains undressed; see, e.g., [38].

(3) We demonstrate the extension of the eikonal-Volkov solutions in the vicinity of the core, where the atomic or molecular potential is no longer a perturbation and the naive eikonal approximation breaks down. We describe approximate regularization procedures for the phase and amplitude and test their accuracy.

(4) The eikonal-Volkov states describe modification of the incident plane wave due to ionic potential, but they do not describe back-scattered wave. We extend the formalism beyond the eikonal approximation to describe large-angle scattering during the electron recollision with the parent ion in the strong laser field.

(5) We show that in the limit of long propagation times the eikonal-Volkov solutions take the form of quasienergy (Floquet) states of the strongly-driven continuum electron in the presence of the ionic core.

(6) We extend the eikonal-Volkov states to describe a strongly driven two-electron continuum and derive both the phase and amplitude of the corresponding two-electron wave functions.

(7) Finally, we address the question of how the resulting rather complicated general expressions for transition amplitudes can be simplified using the saddle-point analysis [39–43] of the corresponding integrals. We stress the connection between the saddle-point equations and classical trajectories that include the atomic or molecular potential perturbatively. We propose an iterative method for solving the saddle point equations, and describe how to use it for one-photon XUV ionization in the presence of strong laser field and for high-harmonic generation.

At this point, the reader may wonder why should one expect the eikonal approximation to be useful for describing electron scattering on a polyatomic target in the strong laser field. Already field-free scattering requires sophisticated approaches to describe resonances and multiple scattering events. The strong field might be expected to add even more complexity to the problem. Indeed, the eikonal continuum functions can only describe small angle scattering, which we refer to as "soft collisions." We refer to large-angle scattering, which classically implies small impact parameters, as "hard collisions."

We show how hard collisions in a strong laser field can be treated using Born-like series while including interaction with the potential partially to all orders. For this purpose, we develop appropriate S-matrix-type expressions, partitioning the Hamiltonian into a short-range part responsible for hard collisions and a long-range part responsible for soft collisions. The resulting Born-like series is in the number of hard collisions with the short range singular part of the target potential. At the same time, soft collisions are treated using the eikonal functions for the long-range nonsingular part of the target potential.

A key aspect of strong-field scattering is that, in general, such Born-like series in the number of hard collisions converge rapidly. Indeed, large-angle scattering typically results in the electron trajectories that do not return to the core. Such scattering yields hot ATI electrons, whose high drift energy $E \gg 2U_p$ prevents the laser field from bringing these electrons back.

The evidence of such convergence is the famous plateau structures in the hot ATI spectra (see, e.g., [44]) and in laser-induced multiphoton bremsstrahlung and inverse bremsstrahlung spectra [45]. The plateau is the result of a highly nonlinear interaction of the electron with the strong infrared laser field and a single hard collision—"recollision" with the target. Manakov *et al.* [45] showed that multiple collisions lead to multiple plateau structures in the electron spectra, each subsequent plateau being several orders of magnitude weaker and shifted to higher energies. Physically, the existence of a single dominating plateau in the ATI spectra means that during electron scattering in a strong laser field the electron experiences only one hard collision. Mathematically, this means that a Born-like series with respect to the scattering potential would converge already after the first term. However, this does not rule out multiple soft collision events (see, e.g., [46] for multiple returns in the SFA), which are well described within the eikonal approximation. Thus it appears that, counter to common intuition, the strong laser field can *simplify* some aspects of scattering.

In the case of shape resonances (see, e.g., [47]) we expect

similar simplifications: The strong laser field with intensities around $I \sim 10^{14}$ W/cm^2 and greater will destroy any resonance continuum structures corresponding to long-lived continuum trajectories around the core. The strong laser field induces large-amplitude (several tens of angstroms for typical IR field intensities) electron oscillations, driving the electron away from the core and liberating the trajectories trapped near the core.

However, we should single out a special case of light induced quasi-bound states. These states are responsible for peculiar intensity-dependent structures in ATI spectra [48–50] associated with the so-called "channel closing." They correspond to low drift energy of the electron, when both trapping and multiple scattering is possible. These states are of the type of light-induced states in the Kramers-Henneberger potential [51] descending from the low-energy continuum with increasing laser intensity. Our approach is not suited for describing these states.

The rest of this paper is organized as follows. In Sec. I, we describe the basic approach to deriving the eikonal-Volkov solutions. In Secs. II and III, we derive the phase and the amplitude corrections to the Volkov wavefunction of the strongly driven electron, which describe the electron interaction with an arbitrary 3D potential in the eikonal approximation. In Sec. IV, we generalize the results to the arbitrary number of continuum electrons, but focus on the two-electron continuum for illustration. In Sec. V, we demonstrate the connection between the eikonal-Volkov states and the corresponding Floquet (quasienergy) solutions. In Sec. VI, we describe applications of these wave functions to above-threshold ionization (ATI), nonsequential double ionization (NSDI), and laser-assisted ionization by attosecond XUV pulses. In Sec. VII, we describe how the general expressions can be simplified to obtain analytical results. Sections VI and VII lay the foundation of the EVA approach.

I. BASIC APPROACH

To describe the continuum dynamics of an electron in the combined potential of the ion and the laser field we shall consider an initial value problem for the time-dependent Schrödinger equation

$$i\hbar \frac{\partial}{\partial t}\Psi(\boldsymbol{r},t) = \hat{H}\Psi(\boldsymbol{r},t), \tag{1}$$

$$\Psi(\boldsymbol{r},T) = \Psi_{\boldsymbol{k}}(\boldsymbol{r}). \tag{2}$$

Here $\hat{H}=\hat{H}_0+\hat{V}_L(t)$ is the full Hamiltonian, which includes interaction with the laser field $\hat{V}_L(t)$ and the atomic Hamiltonian $\hat{H}_0=\hat{\boldsymbol{p}}^2/2+U(\boldsymbol{r})$, where $U(\boldsymbol{r})$ is the potential of the ionic core. The laser field is turned on at $t=T$. Before this moment, the system is in a continuum eigenstate $\Psi_{\boldsymbol{k}}(\boldsymbol{r})$ of $\hat{H}_0$ with an asymptotic momentum $\boldsymbol{k}$. Nonseparable Coulomb-laser dynamics arises for $t>T$, and our goal is to describe the corresponding distortions of $\Psi_{\boldsymbol{k}}(\boldsymbol{r})$.

We solve this problem analytically using the eikonal approximation. This allows us to obtain general solutions for an arbitrary potential. The first step is to make the WKB ansatz (Wentzel-Kramers-Brilliouin) for the solution $\Psi(\boldsymbol{r},t)$

$$\Psi(\boldsymbol{r},t) = P(\boldsymbol{r},t)e^{iS(\boldsymbol{r},t)/\hbar}. \tag{3}$$

Substituting the ansatz Eq. (3) into Eq. (1) and collecting terms of the order of $\hbar^0$ and $\hbar^1$, one obtains the following equations:

$$-\frac{\partial S(\boldsymbol{r},t)}{\partial t} = \frac{1}{2}[\boldsymbol{\nabla} S(\boldsymbol{r},t)]^2 + U(\boldsymbol{r}) + V_L(t), \tag{4}$$

$$S(\boldsymbol{r},T) = S_0(\boldsymbol{r}), \tag{5}$$

$$-\frac{\partial P(\boldsymbol{r},t)}{\partial t} = \frac{1}{2}[\Delta S(\boldsymbol{r},t)]P(\boldsymbol{r},t) + \boldsymbol{\nabla} S(\boldsymbol{r},t)\,\boldsymbol{\nabla}\, P(\boldsymbol{r},t), \tag{6}$$

$$P(\boldsymbol{r},T) = P_0(\boldsymbol{r}). \tag{7}$$

Here P_0 and S_0 are the initial conditions which correspond to the phase and amplitude of $\Psi_{\boldsymbol{k}}(\boldsymbol{r})$ in the WKB approximation. Equation (4) is the Hamilton-Jacobi equation. We shall consider this equation first and then we shall find a solution of Eq. (6) for the amplitude $P(\boldsymbol{r},t)$. In the following, atomic units ($\hbar=e=m_e=1$) are used throughout.

II. PHASE CORRECTION TO THE VOLKOV FUNCTION

A. Eikonal solution for the phase

We seek the solution of Eq. (4) in the following form:

$$S_{\boldsymbol{k},T}(\boldsymbol{r},t) = S^V_{\boldsymbol{k},T}(\boldsymbol{r},t) + G_{\boldsymbol{k},T}(\boldsymbol{r},t), \tag{8}$$

where $S^V_{\boldsymbol{k},T}(\boldsymbol{r},t)$ is the phase of the Volkov function and $G_{\boldsymbol{k},T}(\boldsymbol{r},t)$ is a correction to the Volkov function due to the presence of the potential $U(\boldsymbol{r})$. In the length gauge ($\hat{V}_L=\boldsymbol{\mathcal{E}}_L\boldsymbol{r}$)

$$S^V_{\boldsymbol{k},T}(\boldsymbol{r},t) = \boldsymbol{k}_L(t)\boldsymbol{r} - \frac{1}{2}\int_T^t \boldsymbol{k}_L^2(\tau)d\tau, \tag{9}$$

while in the velocity gauge [$\hat{V}_L=\hat{\boldsymbol{k}}\boldsymbol{A}(t)+\boldsymbol{A}^2(t)/2$]

$$S^V_{\boldsymbol{k},T}(\boldsymbol{r},t) = \boldsymbol{k}\cdot\boldsymbol{r} - \frac{1}{2}\int_T^t \boldsymbol{k}_L^2(\tau)d\tau. \tag{10}$$

Here $\boldsymbol{k}_L(t)=\boldsymbol{k}+\boldsymbol{A}(t)$ is the instantaneous momentum of the electron in the laser field, $\boldsymbol{k}$ is the canonical momentum, which coincides with the asymptotic momentum of field-free state $\Psi_{\boldsymbol{k}}(\boldsymbol{r})$, and $\boldsymbol{A}(t)$ is the vector potential of the laser field $\boldsymbol{\mathcal{E}}_L(t)=-\partial\boldsymbol{A}(t)/\partial t$. The separation of the phases made in Eq. (8) factors out the rapidly oscillating component of the wave function Eq. (3) that comes from the Volkov function $\Psi^V_{\boldsymbol{k},T}(\boldsymbol{r},t)$ [16]

$$\Psi^V_{\boldsymbol{k},T}(\boldsymbol{r},t) = \frac{e^{iS^V_{\boldsymbol{k},T}(\boldsymbol{r},t)}}{(2\pi)^{3/2}}. \tag{11}$$

Substituting Eq. (8) into Eq. (4), one arrives at the following equation for the function $G_{\boldsymbol{k},T}(\boldsymbol{r},t)$

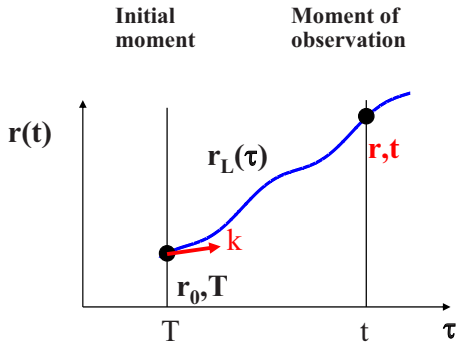

FIG. 1. (Color online) Trajectory given by Eq. (16) is specified by position $\mathbf{r}$ at time t and the asymptotic velocity before the pulse is turned on at $t=T$.

$$-\frac{\partial G_{k,T}(\boldsymbol{r},t)}{\partial t} = \boldsymbol{k}_L \cdot \boldsymbol{\nabla} G_{k,T}(\boldsymbol{r},t) + \frac{1}{2}[\boldsymbol{\nabla} G_{k,T}(\boldsymbol{r},t)]^2 + U(\boldsymbol{r}). \tag{12}$$

This equation has the same form in both length and velocity gauges.

We solve Eq. (12) in the eikonal approximation, by assuming that the change in electron momentum during the scattering event is small

$$|\boldsymbol{\nabla} G_{k,T}(\boldsymbol{r},t)| \ll |\boldsymbol{k}_L(t)|. \tag{13}$$

Neglecting the second term in Eq. (12), we obtain

$$-\frac{\partial G_{k,T}(\boldsymbol{r},t)}{\partial t} = \boldsymbol{k}_L \cdot \boldsymbol{\nabla} G_{k,T}(\boldsymbol{r},t) + U(\boldsymbol{r}). \tag{14}$$

This linear equation can be solved by the method of characteristics [52]. The solution is

$$G^{(\pm)}_{k,T}(\boldsymbol{r},t) = -\int_T^t U(\boldsymbol{r}_L(\tau))d\tau + G^{(\pm)}_{0k}(\boldsymbol{r}_L(T)), \tag{15}$$

$$\boldsymbol{r}_L(\tau) = \boldsymbol{r} + \int_t^\tau \boldsymbol{k}_L(t')dt'. \tag{16}$$

This solution was first obtained by Gersten and Mittleman [33]. We shall refer to $G^{(+)}_{k,T}(\boldsymbol{r},t)$ as the outgoing-type and to $G^{(-)}_{k,T}(\boldsymbol{r},t)$ as the incoming-type continuum solution. This notation is introduced in analogy with the classification of the field-free scattering states [53]: The field-free outgoing and incoming solutions correspond to continuum states, which behave asymptotically like plane waves plus outgoing and incoming spherical waves. The incoming and outgoing-type solutions in Eq. (15) are distinguished by the second term $G^{(\pm)}_{0k}(\boldsymbol{r}_L(T))$ in Eq. (15), associated with the initial condition, as discussed below.

The physics of the result of Eq. (15) is as follows. The first term evaluates the effect of the scattering potential along the trajectory $\boldsymbol{r}_L(\tau)$. This trajectory describes the motion of the electron in the laser field. The trajectory is specified (see Fig. 1) by the position $\boldsymbol{r}$ at the moment of observation t and the initial velocity—the asymptotic momentum $\boldsymbol{k}$ of the initial state $\Psi_k(\boldsymbol{r})$ at the initial moment T.

Introducing the initial coordinate $\boldsymbol{r}_0$

$$\boldsymbol{r}_0 \equiv \boldsymbol{r}_L(T) = \boldsymbol{r} - \int_T^t \boldsymbol{k}_L(t')dt', \tag{17}$$

one can rewrite the trajectory Eq. (16) as

$$\boldsymbol{r}_L(\tau) = \boldsymbol{r}_0 + \int_T^\tau \boldsymbol{k}_L(t')dt'. \tag{18}$$

We stress that $\boldsymbol{r}_0$ depends on time, $\boldsymbol{r}$, $\boldsymbol{k}$, and the laser field parameters.

The second term in Eq. (15) is associated with the initial condition for Eq. (14). This initial condition for $G^{(\pm)}_{k,T}(\boldsymbol{r},t)$ comes from the initial distortion of the field-free continuum state relative to the plane wave [the plane wave contribution $\boldsymbol{k}\cdot\boldsymbol{r}$ is already included into the Volkov phase $S^{(V)}_{k,T}(\boldsymbol{r},t)$]. By definition, the initial condition $G_{0k}(\boldsymbol{r})$ for Eq. (14) is $G_{0k}(\boldsymbol{r}) = S^{(e)}_0(\boldsymbol{r}) - \boldsymbol{k}\cdot\boldsymbol{r}$, where $S^{(e)}_0$ is the phase of the field free electron wave function in the eikonal approximation. That is, $G^{(\pm)}_0(\boldsymbol{r}_L(T))$ is simply given by the initial distortion of the field-free state at the starting coordinate $\boldsymbol{r}_0 \equiv \boldsymbol{r}_L(T)$ [Eq. (17)] of the trajectory $\boldsymbol{r}_L(\tau)$. The signs "$\pm$" correspond to two different kinds of field-free states, corresponding to outgoing ("+") or incoming (−)-type solutions. The field-free initial distortion can be written in a similar way to the first term in Eq. (15), but the integral is taken along the field-free trajectory $\boldsymbol{r}_{\mathrm{FF}}(\tau)$

$$G^{(\pm)}_{0k}(\boldsymbol{r}) = -\int_{\mp\infty}^T U(\boldsymbol{r}_{\mathrm{FF}}(\tau))d\tau, \tag{19}$$

$$\boldsymbol{r}_{\mathrm{FF}}(\tau) = \boldsymbol{r} + \boldsymbol{k}(\tau - T). \tag{20}$$

The outgoing-type initial condition $G^{(+)}_{0k}(\boldsymbol{r})$ corresponds to forward propagation in time from $-\infty$ to T. The incoming-type initial condition $G^{(-)}_{0k}(\boldsymbol{r})$ corresponds to backward propagation in time from ∞ to T. Let us examine Eq. (19) more closely. In the case of $G^{(-)}_{0k}(r)$, introducing the new integration variable $\zeta = \tau - T$ we can rewrite Eq. (19) as follows:

$$G^{(-)}_{0k}(\boldsymbol{r}) = \int_0^{+\infty} U(\boldsymbol{r} + \boldsymbol{k}\zeta)d\zeta. \tag{21}$$

In the case of $G^{(+)}_{0k}(\boldsymbol{r})$, introducing the new integration variable $\xi = T - \tau$ we can rewrite Eq. (19) as follows:

$$G^{(+)}_{0k}(\boldsymbol{r}) = -\int_0^{+\infty} U(\boldsymbol{r} - \boldsymbol{k}\xi)d\xi. \tag{22}$$

In many cases it is convenient to use Cartesian coordinates. For $G^{(+)}_{0k}(\boldsymbol{r})$ we introduce $\boldsymbol{\kappa} = -\boldsymbol{k}$ and assume $|\kappa_z| \geqslant |\kappa_x|, |\kappa_y|$ [54]

$$G_{0\boldsymbol{k}}^{(+)}(x,y,z) = -\frac{1}{\kappa_z}\int_z^{-\infty} dz' U\left(\frac{\kappa_x}{\kappa_z}(z'-z)+x, \frac{\kappa_y}{\kappa_z}(z'-z)+y, z'\right). \tag{23}$$

The upper limit follows from $z'=z-k_z\xi\to-\infty$ for $\xi\to\infty$ for $k_z>0$. Therefore, for $G_{0\boldsymbol{k}}^{(+)}(\boldsymbol{r})$ the flat phase front is in the direction from where the particle comes. For $G_{0\boldsymbol{k}}^{(-)}(\boldsymbol{r})$, assuming $|k_z|\geqslant|k_x|,|k_y|$ we obtain

$$G_{0\boldsymbol{k}}^{(-)}(x,y,z) = -\frac{1}{k_z}\int_{+\infty}^{z} dz' U\left(\frac{k_x}{k_z}(z'-z)+x, \frac{k_y}{k_z}(z'-z)+y, z'\right). \tag{24}$$

The lower limit follows from $z'=z+k_z\zeta\to\infty$ for $\zeta\to\infty$ and $k_z>0$. Therefore, for $G_{0\boldsymbol{k}}^{(-)}(\boldsymbol{r})$ the flat phase front is in the direction where the particle goes.

For a hydrogen atom, Eqs. (23) and (24) yield asymptotic solutions in the so-called Redmond [55] form

$$G_{0\boldsymbol{k}}^{(+)}(\boldsymbol{r}) = -\nu\ln(kr-\boldsymbol{k}\cdot\boldsymbol{r}), \tag{25}$$

$$G_{0\boldsymbol{k}}^{(-)}(\boldsymbol{r}) = \nu\ln(kr+\boldsymbol{k}\cdot\boldsymbol{r}), \tag{26}$$

where $\nu=1/k$ is the Sommerfeld parameter. From now on, we shall omit the superscript $\pm$ in $G_{\boldsymbol{k},T}(\boldsymbol{r},t)$, when we consider the general case relevant for both types of initial conditions.

The initial condition $G_{0\boldsymbol{k}}(\boldsymbol{r})$ ensures continuity of the solutions given by Eq. (15) at $t=T$, when the laser field is turned on. Improper choice of the initial condition would in general degrade the accuracy of the approximation. An arbitrary initial condition $e^{i\tilde{G}_{0\boldsymbol{k}}(\boldsymbol{r})}$ leads to a discontinuity $\Delta(\boldsymbol{r})$ at $t=T$ and $\Delta(\boldsymbol{r})\equiv e^{iG_{0\boldsymbol{k}}(\boldsymbol{r})}-e^{i\tilde{G}_{0\boldsymbol{k}}(\boldsymbol{r})}$. As follows from Eq. (15), this error further propagates along the trajectory given by Eq. (17). For example, starting with plane waves leads to the error $\Delta(\boldsymbol{r})=e^{iG_{0\boldsymbol{k}}(\boldsymbol{r})}-1$. Depending on the type of trajectory $\boldsymbol{r}_L(T)$, the error $\Delta(\boldsymbol{r}_L(T))$ can either propagate away from the interaction area in the case of large drift momenta $k\gg A_0$, or oscillate around it in the case of $k\sim A_0$. Here A_0 is the amplitude of the vector potential of the laser field.

To gauge the accuracy of the approximate solution $G_{\boldsymbol{k},T}(\boldsymbol{r},t)$, we compare it with the solution obtained by exact 1D numerical propagation of the initial WKB continuum wave function $P_w(x)e^{iS_w(x)}$

$$S_w(x,k) = \int^x dx'\sqrt{k^2-2U(x')}, \tag{27}$$

$$P_w(x) = \sqrt{\left|\frac{k}{\partial S_w(x)/\partial x}\right|}, \tag{28}$$

$$U(x) = -1/\sqrt{x^2+a^2}, \tag{29}$$

where $U(x)$ is a soft-core Coulomb potential introduced for laser-matter interaction problems in Ref. [56]. The parameter a is 1.59 a.u., corresponding to the ionization potential I_p of 12.13 eV. The asymptotic field-free momentum is set to $k=1$ a.u. The WKB continuum solution was taken for convenience of having an analytical initial condition. Features in the numerical solution introduced by the approximate initial conditions will be discussed below. The results shown in Fig. 2 are obtained after back propagation in a cw laser field starting with $A(T)=0$ for three periods. The laser intensity is $I=9.3\times10^{12}$ W/cm^2 and wavelength is $\lambda=800$ nm. The coordinate- and time-dependent phase of the Volkov functions is removed from the numerical results for the sake of comparison with the phase $G_{\boldsymbol{k},T}(\boldsymbol{r},t)$. The dashed curve shows the corresponding initial condition $S_w(x,k)-kx$. The solid curves on the upper and lower panels show the numerical and approximate solutions correspondingly.

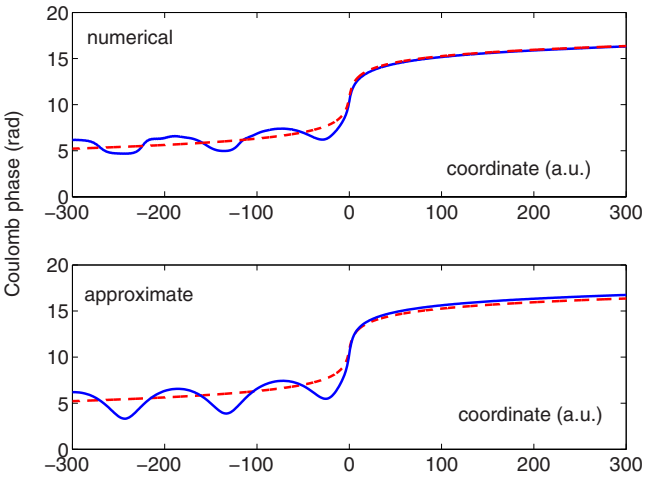

FIG. 2. (Color online) Comparison of the approximate solution for the phase correction induced by a 1D soft-core potential with the exact numerical solution. The coordinate- and time-dependent phase of the Volkov function is subtracted. The results are shown after three periods of propagation in a cw laser field starting with $A(T)=0$, for laser intensity $I=9.3\times10^{12}$ W/cm^2 and wavelength $\lambda=800$ nm. The initial asymptotic momentum is $k=1$ a.u. and electron arrives from $-\infty$. The dashed red curve shows the initial phase.

The approximate and exact numerical solution are similar, but the minima in the approximate solution are more pronounced. The deviations from the numerical solution appear when the oscillating electron passes the core with low velocity and the potential $U(\boldsymbol{r})$ is no longer a perturbation. In this case one can improve the approximate solution by implementing the regularization procedure discussed below.

B. Ranges of applicability and regularizations of the eikonal solution

Strong field dynamics can occur in three distinct regimes. (A) Trajectories $\boldsymbol{r}_L(\tau)$ never pass directly over the core, $|\boldsymbol{\nabla}G_{\boldsymbol{k},T}(\boldsymbol{r},t)|$ is small everywhere, so that $|\boldsymbol{\nabla}G_{\boldsymbol{k},T}(\boldsymbol{r},t)|\ll|\boldsymbol{k}_L(t)|$ even when $|\boldsymbol{k}_L(t)|$ is small. (B) Trajectories $\boldsymbol{r}_L(\tau)$ can pass near the core. In this case $|\boldsymbol{\nabla}G_{\boldsymbol{k},T}(\boldsymbol{r},t)|$ can be large, but $|\boldsymbol{k}_L(t)|$ is still larger: $|\boldsymbol{\nabla}G_{\boldsymbol{k},T}(\boldsymbol{r},t)|\ll|\boldsymbol{k}_L(t)|$. (C) Trajectories $\boldsymbol{r}_L(\tau)$ can pass near the core, $|\boldsymbol{\nabla}G_{\boldsymbol{k},T}(\boldsymbol{r},t)|$ is large near the core, and may become large compared to $|\boldsymbol{k}_L(t)|$.

For example, dynamics of the so-called direct electrons produced by strong-field ionization occurs in regime (A). The electrons produced via one-photon XUV ionization in the presence of a strong laser field fall within regime (B). This regime also arises during the recombination step of high-energy harmonic generation in strong laser fields.

The electron dynamics in strong field processes involving recollision in general belongs to the most general regime (C).

Regimes (A) and (B) are both within the applicability of the eikonal approximation. In case (A), the eikonal solution does not require any regularizations since local divergencies appear only when the trajectory passes through the core. Regime (B) requires regularization near local divergencies. In regime (C), the eikonal solutions cannot be applied directly, since Eq. (13) is not always satisfied. A possible way to deal with this complication is described in Sec. VI C.

Now we describe the regularization procedure relevant for regime (B). For this combination of parameters, the electron has a large drift velocity and it will leave "the interaction area" before its instantaneous momentum $|\boldsymbol{k}_L(t)|$ has a chance to change significantly due to the laser field. Therefore, one can assume that the laser field supplies the asymptotic momentum $\boldsymbol{k}_L(t)$ and then apply the regularization procedure as if we were dealing with an autonomous system. For an autonomous system the natural regularization of the eikonal solution is the WKB action $S_{\mathrm{WKB}}(\boldsymbol{r},\boldsymbol{k})=\int dl\sqrt{k^2-2U[\boldsymbol{r}(l)]}$, where dl implies integration along the electron trajectory $\boldsymbol{r}(l)$. Indeed, the eikonal approximation is equivalent to the perturbative expansion of the WKB action in powers of potential $U(\boldsymbol{r}):S_{\mathrm{WKB}}(\boldsymbol{r},\boldsymbol{k})\simeq\boldsymbol{k}\cdot\boldsymbol{r}-\int dl\, U[\boldsymbol{r}(l)]/k$. This expansion is applicable only if the interaction with the potential can be considered as a small perturbation. Near the core the expansion diverges and therefore the original formula $S_{\mathrm{WKB}}(\boldsymbol{r},\boldsymbol{k})=\int dl\sqrt{k^2-2U[\boldsymbol{r}(l)]}$ should be used: $\int dl\, U[\boldsymbol{r}(l)]/k\to\int dl[k-\sqrt{k^2-2U[\boldsymbol{r}(l)]}]$.

Returning to the non-autonomous system, the WKB action in the adiabatic approximation is $S^{\mathrm{ad}}_{\mathrm{WKB}}(\boldsymbol{r},\boldsymbol{k})=\int dl\sqrt{k_L(t)^2-2U[\boldsymbol{r}(l,t)]}$, with the integral performed along the eikonal trajectory: $dl=k_L(t)dt$. Therefore, the appropriate regularization of $G_{k,T}(\boldsymbol{r},t)$ is to replace it with $\sigma_{k,T}(\boldsymbol{r},t)$

$$\sigma_{k,T}(\boldsymbol{r},t)=-\int_T^t dt' k_L(t')[k_L(t')-\sqrt{k_L(t')^2-2U[\boldsymbol{r}_L(t')]}]. \tag{30}$$

Equation (30) regularizes the solution near the origin and yields correct results away from the origin. Indeed, in the strong-field limit, where the laser-induced motion dominates the Coulomb potential, one may assume that $k_L^2\gg U$. Then the expansion of $\sigma_{k,T}(\boldsymbol{r},t)$ in Eq. (30) reduces back to $G_{k,T}(\boldsymbol{r},t)$

$$\sigma_{k,T}(\boldsymbol{r},t)|_{k_L^2\gg U}\approx-\int_T^t dt' U[\boldsymbol{r}_L(t')]=G_{k,T}(\boldsymbol{r},t).$$

At the same time, in the weak field limit $k_L(t')\approx k$, the integral Eq. (30) simply yields the standard WKB expression for the contribution of the Coulomb potential to the coordinate-dependent phase of the WKB wave function

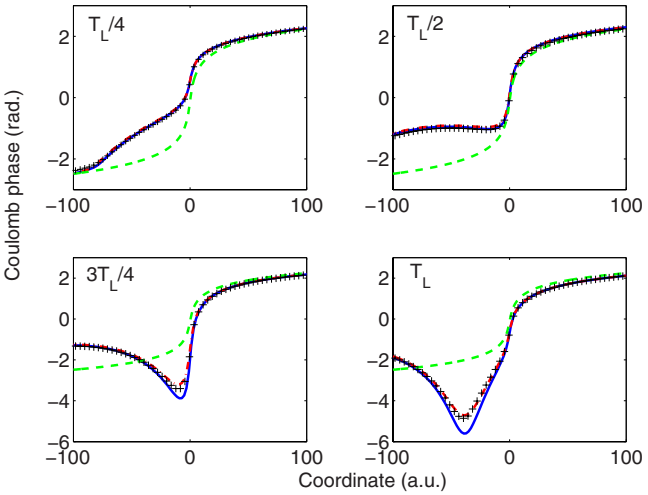

FIG. 3. (Color online) Comparison of different approximations for the phase correction induced by a 1D soft-core potential with the numerical solution (crosses). The coordinate- and time-dependent phase of Volkov function is subtracted. The results are shown after quarter, half, three quarters, and one period of propagation in cw laser field starting with $A(T)=0$, for laser intensity $I=1.5\times10^{14}$ W/cm^2 and wavelength $\lambda=800$ nm. The initial asymptotic momentum is $k=2$ a.u. The dashed green curve shows the initial Coulomb phase. Blue solid line shows nonregularized phase $G_{k,T}(x,t)$; red dash-dotted curve shows regularized phase $\sigma_{k,T}(x,t)$.

$$\sigma_{k,T}(\boldsymbol{r},t)|_{k_L\approx k}\approx-\int_T^t dt'[k-\sqrt{k^2-2U[\boldsymbol{r}_L(t')]}]k$$
$$=\int_{r_0}^{r} dl\sqrt{k^2-2U[\boldsymbol{r}(l)]}-\boldsymbol{k}\cdot\boldsymbol{r}+\boldsymbol{k}\cdot\boldsymbol{r}_0.$$

Figure 3 shows that the regularized solution is indeed much more accurate. We have considered the same 1D model as in Fig. 2 above. We stress that this regularization procedure should not be used in regime (A), not only because it is not required, but also due to the nonadiabatic character of electron dynamics in regime (A). Using regularization procedure described above in regime (A) would yield incorrect results.

C. Adiabatic approximation to the phase of the eikonal-Volkov solution

It is instructive to consider the adiabatic approximation (see, e.g., Ref. [36]) to the eikonal-Volkov solutions. This approximation greatly simplifies both numerical and analytical calculations. The adiabatic approximation replaces the electron trajectory in the laser field $\boldsymbol{r}_L(\tau)$ in Eq. (15) with the adiabatic trajectory $\boldsymbol{r}_{\mathrm{ad}}(\tau)$

$$\boldsymbol{r}_{\mathrm{ad}}(\tau)=\boldsymbol{r}+\boldsymbol{k}_L(t)(\tau-t). \tag{31}$$

Specifically, the adiabatic approximation is done in the integral Eq. (16) by taking $\boldsymbol{k}_L(t')$ out of the integral at $t'=t$

$$\int_t^\tau \boldsymbol{k}_L(t')dt' \simeq \boldsymbol{k}_L(t)(\tau - t). \tag{32}$$

Physically, this approximation assumes that the electron momentum does not change while the electron passes near the core, where the eikonal phase is significant. The adiabatic approximation to the phase given by Eq. (15) is

$$G_{k,T}^{\mathrm{ad(eV)}}(\boldsymbol{r},t) = -\int_T^t U(\boldsymbol{r}_{\mathrm{ad}}(\tau))d\tau + G_{0\boldsymbol{k}}^{(\pm)}(\boldsymbol{r}_{\mathrm{ad}}(T)). \tag{33}$$

This approximation is justified for high energy electrons in regime (B), but is not justified in regimes (A) and (C) (see Sec. VI).

D. Strong field limit

In the strong field limit, when the motion of the electron is dominated by oscillations rather then the drift motion, the Coulomb phase accumulated during each period has a double-peak structure. Each peak is accumulated at the turning points of the electron trajectory. Indeed, the Coulomb phase accumulated during one period for $k=0$ is related to the Kramers-Henneberger potential U_{KH} [51]

$$-\int_{-2\pi/\omega}^{0} d\tau\, U\left[r + \int_0^\tau \boldsymbol{A}(t')dt'\right] \equiv \frac{U_{\mathrm{KH}}}{\omega}. \tag{34}$$

The Kramers-Henneberger potential acquires a double-well structure when the amplitude of the electron oscillations is larger than the characteristic size of the potential.

III. CORRECTION TO THE AMPLITUDE OF THE VOLKOV FUNCTION

The standard eikonal approximation only involves the phase corrections Eq. (15) to the wave-function of the free electron (see, e.g., [30] for the laser field-free case and [33] for field-dressed case). The amplitude corrections derived below improve the standard eikonal approximation in the way similar to the generalized eikonal approximation introduced in Ref. [34].

In this section we consider Eq. (6) for the wavefunction amplitude. This equation can be solved for an arbitrary classical action $S(\boldsymbol{r},t)$ as soon as one takes into account the relationship between the classical action and the corresponding momentum $\boldsymbol{p}(\boldsymbol{r},t)$

$$\nabla S(\boldsymbol{r},t) = \boldsymbol{p}(\boldsymbol{r},t). \tag{35}$$

Then Eq. (6) can be rewritten as

$$\frac{dP^2(\boldsymbol{r},t)}{dt} = -\operatorname{div}\boldsymbol{p}\, P^2(\boldsymbol{r},t). \tag{36}$$

Now, using the Liouville formulas, $\operatorname{div}\boldsymbol{p} = (d/dt)\ln J$, we get

$$P(\boldsymbol{r},t) = \frac{P_0(\boldsymbol{r}_0)}{\sqrt{|J|}}, \tag{37}$$

where $J = \det|\partial(\boldsymbol{r}(t))/\partial(\boldsymbol{r}_0)|$ is the Jacobian relating a current coordinate on the trajectory $\boldsymbol{r}(t)$ given by the equation of motion $d\boldsymbol{r}(t)/dt = \boldsymbol{p}(\boldsymbol{r},t)$ with the initial coordinate $\mathbf{r}_0$ at the moment T.

Equation (37) gives the first term in the $\hbar$ expansion of the amplitude of the exact wave function. However, Eq. (37) can only be approached numerically, since there is no analytical expression for the trajectory $\boldsymbol{r}(t)$. Thus it is important to find reliable approximations to Eq. (37).

Using Eqs. (8) and (35), we obtain the momentum and the corresponding trajectory in the eikonal approximation

$$p^e(\boldsymbol{r},t) = \nabla S^e(\boldsymbol{r},t) = \boldsymbol{k}_L(t) + \nabla G_{k,T}(\boldsymbol{r},t), \tag{38}$$

$$\boldsymbol{r}^e(t) = \boldsymbol{r}_0 + \int_T^t \boldsymbol{k}_L(\tau)d\tau - \int_T^t d\tau \int_T^\tau dt' \times \nabla U\left[\boldsymbol{r}_0 + \int_T^{t'} \boldsymbol{k}_L(t'')dt''\right]. \tag{39}$$

The trajectory $\boldsymbol{r}_L(\tau)$ in the argument of the potential $U(\boldsymbol{r})$ is taken in the form suggested by Eq. (18). This is essential for calculating the amplitude, which is defined via $\partial(\boldsymbol{r}(t))/\partial(\boldsymbol{r}_0)$. That is, for this calculation $\boldsymbol{r}_0$ is treated as an independent variable while $\boldsymbol{r}(t)$ depends on it. This is the reason why the initial phase $G_{0\boldsymbol{k}}(\boldsymbol{r}_0)$ does not contribute to Eq. (38).

Now we are in a position to calculate the Jacobian. Keeping only terms of the zeroth and first order with respect to the binding potential $U(\boldsymbol{r})$, we obtain the Jacobian in the eikonal approximation

$$J^e = 1 - \int_T^t dt' \int_T^{t'} d\,\tau \Delta U\left[\boldsymbol{r} + \int_t^\tau \boldsymbol{k}_L(t'')dt''\right]. \tag{40}$$

Thus the amplitude in the eikonal approximation is

$$P^e(\boldsymbol{r},t) = \frac{P_0(\boldsymbol{r}_0)}{\sqrt{\left|1 - \int_T^t dt' \int_T^{t'} d\tau \Delta U[\boldsymbol{r}_L(\tau)]\right|}}, \tag{41}$$

where $\boldsymbol{r}_L(\tau)$ and $\boldsymbol{r}_0$ are given by Eqs. (16) and (17).

The double integral can be further simplified in the adiabatic approximation, assuming that the electron instantaneous momentum $\boldsymbol{k}_L(t)$ does not change significantly while the electron passes the interaction area. We first rewrite Eq. (40) as

$$J^{(e)} = 1 + \int_T^t dt' I(\boldsymbol{r},t'), \tag{42}$$

where

$$I(\boldsymbol{r},t') = -\int_T^{t'} d\tau\, \Delta U[\boldsymbol{r}_L(\tau)]. \tag{43}$$

Let us introduce an auxiliary variable $\tilde{\boldsymbol{k}}_C$:

$$\tilde{\boldsymbol{k}}_C(t',\boldsymbol{r}) = -\int_T^{t'} d\tau\, \nabla U[\boldsymbol{r}_L(\tau)]. \tag{44}$$

Differentiating Eq. (44) twice with respect to t' we obtain

$$-\Delta U(\boldsymbol{r}_L(t'))\boldsymbol{k}_L(t') = \frac{d^2\tilde{\boldsymbol{k}}_C}{dt'^2}. \tag{45}$$

Multiplying both parts of Eq. (45) by $\boldsymbol{k}_L(t')$ we deduce

$$-\Delta U(\boldsymbol{r}_L(t')) = \frac{\boldsymbol{k}_L(t')}{|\boldsymbol{k}_L(t')|^2}\frac{d^2\tilde{\boldsymbol{k}}_C}{dt'^2}. \tag{46}$$

Substituting Eq. (46) into Eq. (43) and integrating by parts we obtain

$$I(\boldsymbol{r},t') = \left|\frac{\boldsymbol{k}_L(\tau)}{|\boldsymbol{k}_L(\tau)|^2}\frac{d\tilde{\boldsymbol{k}}_C(\tau)}{d\tau}\right|_T^{t'} - \int_T^{t'}\frac{d\tilde{\boldsymbol{k}}_C(\tau)}{d\tau}d\left[\frac{\boldsymbol{k}_L(\tau)}{|\boldsymbol{k}_L(\tau)|^2}\right]$$

$$\simeq \frac{\boldsymbol{k}_L(t')}{|\boldsymbol{k}_L(t')|^2}\frac{d\tilde{\boldsymbol{k}}_C(t')}{dt'}. \tag{47}$$

Here we (i) simplified the first term taking into account that $d\tilde{\boldsymbol{k}}_C(T)/dT = \nabla U[\boldsymbol{r}_0] \to 0$ for $\boldsymbol{r}_0 \to \infty$ and (ii) neglected the second term assuming the adiabatic approximation. Substituting Eq. (47) into Eq. (42) and repeating the procedure and the argument above, we obtain

$$J^e - 1 = \frac{\boldsymbol{k}_L(t')\tilde{\boldsymbol{k}}_C(t')}{|\boldsymbol{k}_L(t')|^2}\left|_T^t - \int_T^t \tilde{\boldsymbol{k}}_C(t')d\left[\frac{\boldsymbol{k}_L(t')}{|\boldsymbol{k}_L(t')|^2}\right]\right.$$

$$\simeq \frac{\boldsymbol{k}_L(t)\tilde{\boldsymbol{k}}_C(t)}{|\boldsymbol{k}_L(t)|^2}. \tag{48}$$

To arrive to the final result we note that the auxiliary quantity $\tilde{\boldsymbol{k}}_C$ introduced above is related to the momentum $\boldsymbol{k}_C(t) \equiv \nabla G_{k,T}(\boldsymbol{r},t)$ acquired due to the interaction with the potential in the eikonal approximation

$$\tilde{\boldsymbol{k}}_C(t) = \boldsymbol{k}_C(t). \tag{49}$$

Therefore, the adiabatic approximation for the amplitude in the eikonal approximation yields

$$P^{\mathrm{ad}}(\boldsymbol{r},t) = P_0(\boldsymbol{r}_0)\left|1 + \frac{\boldsymbol{k}_L(t)\boldsymbol{k}_C(t)}{|\boldsymbol{k}_L(t)|^2}\right|^{-1/2}, \tag{50}$$

where $\boldsymbol{r}_0 = \boldsymbol{r}_L(T)$ is the time-dependent function given by Eq. (17). Note that Eq. (50) can be interpreted as a result of the expansion of $P^{\mathrm{ad}}_{\mathrm{WKB}}$

$$P^{\mathrm{ad}}_{\mathrm{WKB}}(\boldsymbol{r},t) = P_0(\boldsymbol{r}_0)\sqrt{\left|\frac{\boldsymbol{k}_L(t)}{\nabla S(\boldsymbol{r},t)}\right|} \tag{51}$$

in powers of $|\boldsymbol{k}_C(t)|$ [57]. Indeed, taking into account that $\nabla S(\boldsymbol{r},t) = \boldsymbol{k}_L(t) + \boldsymbol{k}_C(t)$ and treating $\boldsymbol{k}_C(t)$ perturbatively yields the result of Eq. (50)

$$\sqrt{\left|\frac{\boldsymbol{k}_L(t)}{\boldsymbol{k}_L(t)+\boldsymbol{k}_C(t)}\right|} \simeq \left|1 + \frac{\boldsymbol{k}_L(t)\boldsymbol{k}_C(t)}{|\boldsymbol{k}_L(t)|^2}\right|^{-1/2}. \tag{52}$$

Note, that in the 1D case Eq. (50) immediately yields

$$P^{\mathrm{ad}}(x,t) = P_0(x_0)\sqrt{\left|\frac{k_L(t)}{k_L(t)+k_C(t)}\right|}, \tag{53}$$

where $x_0 = x_L(T)$.

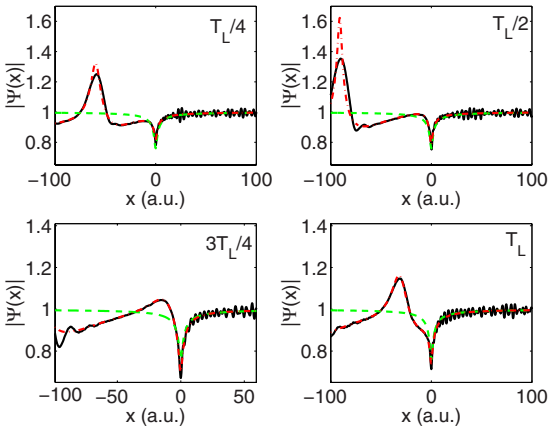

FIG. 4. (Color online) Comparison of the WKB amplitude Eq. (37) with the numerical solution (solid line). The results are shown after quarter, half, three quarters, and one period $T_L = 2\pi/\omega$ of propagation in cw laser field starting with $A(T)=0$, for laser intensity $I = 10^{13}$ W/cm^2 and wavelength $\lambda = 800$ nm. The initial asymptotic momentum is $k=1$ a.u. Dashed (green) curve shows the initial WKB amplitude Eq. (55). Solid (black) curve shows the electron density evaluated numerically. Dash-dotted (red) curve shows the WKB amplitude.

The initial amplitude $P_0(\boldsymbol{r})$ can be obtained from $P(\boldsymbol{r},t)$ as a stationary solution in the limit $\lim_{T-\tilde{T}\to\infty} P(\boldsymbol{r},T)$ corresponding to zero field and satisfying the initial condition $P(\boldsymbol{r},\tilde{T}) = 1$ $(T > \tilde{T})$. In this case Eq. (40) takes the form

$$J^e = 1 - \int_{\tilde{T}}^{T} dt' \int_{\tilde{T}}^{t'} d\tau\, \Delta U[\boldsymbol{r} + \boldsymbol{k}\cdot(T-\tau)] \tag{54}$$

and the limit $T - \tilde{T} \to \infty$ yields the initial amplitude in the eikonal approximation

$$P_0^e(\boldsymbol{r}) = \left|1 - \frac{U(\boldsymbol{r})}{k^2}\right|^{-1/2}. \tag{55}$$

As it can be seen from the definition of the adiabatic amplitude Eq. (50), the same initial amplitude Eq. (55) applies in this case.

To check the accuracy of the different approximate solutions for the amplitude, we compare them with the numerical solution. The solution corresponds to back-propagation in time of the initial field-free state Eqs. (27) and (28) with positive momentum $k=1$ a.u. We first discuss the numerical solution, then the WKB amplitude Eq. (37) and finally the approximations to the WKB amplitude Eqs. (41) and (51).

The numerically calculated amplitude and the WKB amplitude are shown in Fig. 4 after quarter, half, three quarters, and one period of propagation in cw laser field starting with $A(T)=0$, for laser intensity $I = 10^{13}$ W/cm^2 and wavelength $\lambda = 800$ nm. The dashed curve in Fig. 4 shows that the initial electron density Eq. (28) drops near the origin of the potential $U(\boldsymbol{r})$, since the electron is accelerated and spends less time near the origin. The solid curve represents the numerical solution for the electron density. The electron density near the core evolves periodically in time. It drops near the origin,

has a peak away from the origin, and rapid oscillations, which are the most prominent for $x>0$. These oscillations are artifacts related to the choice of the WKB solution as the initial condition for the numerical simulation. Increasing the initial momentum one improves the quality of this approximation. The artifacts gradually disappear in our simulations with increasing k, as expected. The peak in the electron density appears periodically, once per cycle, near the origin (see $t=3T_L/4$, in Fig. 4), and then propagates away from the origin (see $t=T_L$, $t=T_L/4$, $t=T_L/2$ in Fig. 4). Note $T_L/2$ ($T_L=2\pi/\omega$) phase-lag of the amplitude with respect to the phase (Fig. 3).

This peak in the density reflects the electron bunching after scattering. Since electrons that scatter from the core at different times have different momenta $\boldsymbol{k}_L(t)$ at the moment of scattering, they will change their energy in different ways: some slow down and some speed up. This leads to electron bunching: fast electrons that scattered later catch up with the slow electrons that scattered earlier.

The dash-dotted line in Fig. 4 shows the WKB amplitude, calculated according to Eq. (37) using numerically evaluated trajectories $x(t,x_0)$ for 2000 different initial coordinates x_0 and the corresponding initial momenta $p_0=\sqrt{k^2-2U(x_0)}$, $k=1$ a.u. The potential $U(x)$ has been specified above [see Eqs. (27) and (28)]. The WKB solution for the amplitude are in a good agreement with the numerical solution near the origin, but increasingly overestimate the electron bunching far from the core while the "bunch" propagates away (see $t=T_L/4$ and $t=T_L/2$ in Fig. 4).

Physically, the origin of this discrepancy lays in the quasiclassical nature of the approximate solution. The numerical solution is fully quantum and therefore the Heisenberg uncertainty relation ultimately limits the shrinking of the electron bunch. The WKB amplitude Eq. (37) represents only the first term in the $\hbar$ expansion of the electron density and does not completely reflect the wave nature of the electron.

Note that the deficiency in the WKB amplitude arises far from the core, i.e., away from the most important region where photo-excitation or strong-field ionization takes place.

Mathematically, the origin of the discrepancy is a breakdown of the approximation for $J(x_0,t)=0$. In optics, the corresponding manifold $\{x_0,t\}$ defines the caustic and the corresponding points on the trajectory $x=x(t,x_0)$ are the focal points.

Figure 5 shows the trajectory $x=x(T_L,x_0)$ as a function of initial coordinate, and its derivative $dx(T_L,x_0)/dx_0$, at $t=T_L=2\pi/\omega$. The caustic appears at $x_0\simeq 200$ a.u. [Fig. 5(b)] and the focal point is $x\simeq -130$ a.u. [Fig. 5(a)]. Note, that all features of the WKB amplitude (Fig. 4, $t=T_L$) can be traced back to the derivative $dx(T_L,x_0)/dx_0$ as soon as we map x_0 into x using the upper panel of Fig. 5. The spike in the derivative at $x_0\simeq 330$ a.u. translates into the drop of the WKB amplitude near the origin, the local drop of the derivative near $x_0\simeq 305$ a.u. translates into the hump in the WKB amplitude near $x\simeq -30$ a.u. There are different approaches that allow one to regularize the local divergencies of the WKB amplitude [58,59], but this subject is outside the scope of the present work.

Now we discuss the accuracy of our approximations to Eq. (37). The dash-dotted curve in Fig. 6 shows that the

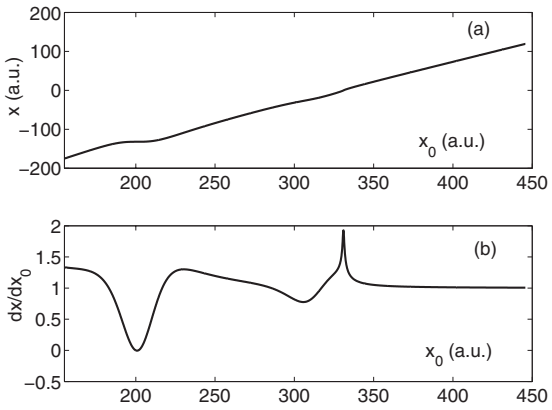

FIG. 5. (a) Numerically evaluated electron trajectory is plotted as a function of initial coordinate x_0 at $t=T_L$. The focal point is $x=-130$ a.u. (b) To illustrate the appearance of caustics we plot the derivative of the trajectory with respect to the initial coordinate x_0. The caustic appears at $x_0\simeq 200$ a.u., when the derivative is equal to zero.

eikonal approximation for the amplitude [Eq. (41)] strongly overestimates electron bunching. The reason is that the eikonal approximation cannot provide the same accuracy for slow and fast electrons.

However, this problem does not appear in the case of the adiabatic amplitude (dotted curve in Fig. 6): In the adiabatic approximation electron bunching does not occur. Indeed, the height of the peak in the adiabatic approximation is the same for different moments of time. All three approximations are satisfactory near the core, which is the most important region for most strong field problems.

To summarize, we have considered three different approximations for the wave function amplitude $P(\boldsymbol{r},t)$ of Eq.

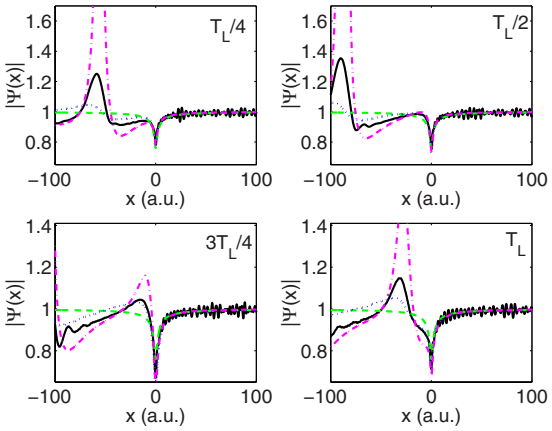

FIG. 6. (Color online) Comparison of different approximations for the amplitude with the numerical solution (solid line). The results are shown after quarter, half, three quarters, and one period of propagation in cw laser field starting with $A(T)=0$, for laser intensity $I=10^{13}$ W/cm^2 and wavelength $\lambda=800$ nm. The initial asymptotic momentum is $k=1$ a.u. Dashed (green) curve shows the initial WKB amplitude Eq. (55). Solid (black) curve shows the electron density evaluated numerically. Dash-dotted (magenta) curve shows the eikonal amplitude Eq. (41). Dotted (blue) curve shows the adiabatic approximation for the amplitude Eq. (51).

(3). The WKB amplitude Eq. (37) is the first term in an $\hbar$ expansion of the amplitude of the exact wave function. The eikonal amplitude Eq. (41) is the first term in the expansion of the WKB amplitude $P(\boldsymbol{r},t)$ in powers of the potential $U(\boldsymbol{r})$. The adiabatic amplitude Eq. (51) is an approximation to the eikonal amplitude, which assumes that the electron leaves the area of interaction with the potential before its instantaneous momentum $\boldsymbol{k}_L(t)$ is changed substantially due to the laser field. All of these approximations work well near the core. The adiabatic amplitude is the most convenient for applications, since it avoids difficulties of describing electron bunching and is the easiest to calculate.

IV. TWO-ELECTRON CONTINUUM

The approximate solutions obtained above can be generalized to include many interacting electrons in the continuum.

Consider two electrons. The full Hamiltonian is $\hat{H}=\hat{H}_{01}+\hat{H}_{02}+\hat{V}_L+\hat{V}^{ee}$, where $\hat{H}_{01}$ and $\hat{H}_{02}$ describe the interaction of each of the electrons with the binding potential $U(\boldsymbol{r})$, $\hat{V}^{ee}$ describes the interaction between the electrons, and $\hat{V}_L$ describes the interaction of both electrons with the laser field. We make the following eikonal ansatz for the solution of Eq. (4)

$$S(\boldsymbol{r}_1,\boldsymbol{r}_2,t)=S_1(\boldsymbol{r}_1,t)+S_2(\boldsymbol{r}_2,t)+G_{12}(\boldsymbol{r}_1,\boldsymbol{r}_2,t), \tag{56}$$

$$S_1(\boldsymbol{r}_1,t)=S^V_{\boldsymbol{k}1,T}(\boldsymbol{r}_1,t)+G_{\boldsymbol{k}1,T}(\boldsymbol{r}_1,t), \tag{57}$$

$$S_2(\boldsymbol{r}_2,t)=S^V_{\boldsymbol{k}2,T}(\boldsymbol{r}_2,t)+G_{\boldsymbol{k}2,T}(\boldsymbol{r}_2,t). \tag{58}$$

$S^V_{\boldsymbol{k}_j,T}(\boldsymbol{r}_j,t)$ is the one-electron Volkov phase and $G_{\boldsymbol{k}_j,T}(\boldsymbol{r}_j,t)$ is the one-electron eikonal correction to this phase obtained above; see Eq. (15).

Substituting Eq. (56) into Eq. (4) yields, in the eikonal approximation,

$$-\frac{\partial G_{12}}{\partial t}=\boldsymbol{k}_{L1}\boldsymbol{\nabla}_1 G_{12}+\boldsymbol{k}_{L2}\boldsymbol{\nabla}_2 G_{12}+V^{ee}(\boldsymbol{r}_1-\boldsymbol{r}_2). \tag{59}$$

Here $\boldsymbol{k}_{L1}=\boldsymbol{k}_1+\boldsymbol{A}(t)$ and $\boldsymbol{k}_{L2}=\boldsymbol{k}_2+\boldsymbol{A}(t)$ are the instantaneous momenta of each electron, while $\boldsymbol{k}_1$ and $\boldsymbol{k}_2$ are the corresponding asymptotic momenta. This equation and its solution do not depend on the laser field, since the relative coordinate of the two electrons $\boldsymbol{r}_{12}=\boldsymbol{r}_1-\boldsymbol{r}_2$ is not affected by the laser field. Introducing the relative momentum $\Delta\boldsymbol{k}=\boldsymbol{k}_1-\boldsymbol{k}_2$, we obtain

$$G^{(\pm)}_{12,\Delta\boldsymbol{k}}(\boldsymbol{r}_{12})=-\int_{\mp\infty}^{t} d\tau\, V_{12}[\boldsymbol{r}_{12}+\Delta\boldsymbol{k}(\tau-t)]. \tag{60}$$

The lower limit in the integral is changed from T to $-\infty$, incorporating the initial condition. Equation (60) can be rewritten as

$$G^{(\pm)}_{12,\Delta\boldsymbol{k}}(\boldsymbol{r}_{12})=\pm\int_0^{\infty} d\tau\, V_{12}(\boldsymbol{r}_{12}\mp\Delta\boldsymbol{k}\tau). \tag{61}$$

Note that $G^{(-)}_{12,\Delta\boldsymbol{k}}$ corresponds to the solution that approaches a plane wave at large relative coordinate r_{12} *in the direction of the relative electron momentum* $\Delta\boldsymbol{k}$. In the opposite direction, parallel to $-\Delta\boldsymbol{k}$, the wave front curvature increases with increasing electron-electron separation r_{12}. $G^{(+)}_{12,\Delta\boldsymbol{k}}$ corresponds to the solution that approaches a plane wave at large relative coordinate r_{12} *in the direction opposite to the relative electron momentum* $\Delta\boldsymbol{k}$. As it was discussed above [see Eqs. (25) and (26)], Eq. (61) leads to the Redmond asymptotic form [55]

$$G^{(\pm)}_{12,\Delta\boldsymbol{k}}(\boldsymbol{r}_{12})=\pm\nu\ln[\mp\Delta\boldsymbol{k}\cdot\boldsymbol{r}_{12}+\Delta k r_{12}], \tag{62}$$

where $\nu=1/\Delta k$ is the analog of the Sommerfeld parameter.

To obtain the amplitude of the two-electron wave function, one can still use Eqs. (16) and (37), keeping in mind that now the Jacobian matrix is 6×6 instead of 3×3. In the eikonal approximation the Jacobian yields

$$\begin{aligned} J^e=1&-\int_T^t dt'\int_T^{t'} d\tau\,\Delta_{\boldsymbol{r}_1}U[\boldsymbol{r}_{1L}(\tau)]\\ &-\int_T^t dt'\int_T^{t'} d\tau\,\Delta_{\boldsymbol{r}_2}U[\boldsymbol{r}_{2L}(\tau)]\\ &-\int_T^t dt'\int_T^{t'} d\tau\,2\Delta_{\boldsymbol{r}_{12}}V^{ee}[\boldsymbol{r}_{12}+\Delta\boldsymbol{k}(\tau-t)]. \end{aligned} \tag{63}$$

In the last term we used for the Laplacian $\Delta=\Delta_{\boldsymbol{r}_1}+\Delta_{\boldsymbol{r}_2}$ and $\Delta V^{ee}=2\Delta_{\boldsymbol{r}_1}V^{ee}=2\Delta_{\boldsymbol{r}_2}V^{ee}=2\Delta_{\boldsymbol{r}_{12}}V^{ee}$. Note the absence of the terms associated with initial conditions—the field-free integrals from $-\infty$ to T. The reason is exactly the same as in the one-electron case (see previous section).

The electron trajectories are analogous to the one-electron case ($j=1,2$)

$$\boldsymbol{r}_{jL}(\tau)=\boldsymbol{r}_j+\int_t^{\tau}\boldsymbol{k}_{jL}(t')dt'. \tag{64}$$

Introducing the momenta corresponding to the motion in each of the potentials

$$\boldsymbol{k}_{Cj}(\boldsymbol{r}_j,t)=-\int_T^t d\tau\,\boldsymbol{\nabla}_{\boldsymbol{r}_j}U[\boldsymbol{r}_{jL}(\tau)], \tag{65}$$

$$\boldsymbol{k}_{12}(\boldsymbol{r}_1,\boldsymbol{r}_2,t)=-\int_T^t d\tau\,\boldsymbol{\nabla}_{\boldsymbol{r}_{12}}V^{ee}[\boldsymbol{r}_{12}+\Delta\boldsymbol{k}(\tau-t)], \tag{66}$$

and applying the same method as in the one-electron case considered above, we obtain for the amplitude in the adiabatic approximation

$$P^{\mathrm{ad}}(\boldsymbol{r}_1,\boldsymbol{r}_2,t)=\frac{P_0(\boldsymbol{r}_{10},\boldsymbol{r}_{20})}{|1+A^e_1+A^e_2+A^e_{12}|^{1/2}}, \tag{67}$$

$$A^e_1(\boldsymbol{r}_1,t)=\frac{\boldsymbol{k}_{L1}(t)\boldsymbol{k}_{C1}(t)}{|\boldsymbol{k}_{L1}(t)|^2}, \tag{68}$$

$$A^e_2(\boldsymbol{r}_2,t)=\frac{\boldsymbol{k}_{L2}(t)\boldsymbol{k}_{C2}(t)}{|\boldsymbol{k}_{L2}(t)|^2}, \tag{69}$$

$$A_{12}^{e}(\boldsymbol{R},t) = 2\frac{\Delta\boldsymbol{k}\cdot\boldsymbol{k}_{12}(t)}{|\Delta\boldsymbol{k}|^2}. \tag{70}$$

Here the initial coordinates $\boldsymbol{r}_{10}$ and $\boldsymbol{r}_{20}$ are defined as in the one-electron case [see Eq. (17)] $\boldsymbol{r}_{10}=\boldsymbol{r}_{1L}(T)$ and $\boldsymbol{r}_{20}=\boldsymbol{r}_{2L}(T)$. Note that the coefficient 2 in Eq. (70) appears since the reduced mass of two electrons is $1/2$.

Since in the eikonal approximation one keeps only the first-order terms in powers of the binding potential $U(\boldsymbol{r})$ and the electron-electron interaction potential $V^{ee}(\boldsymbol{r}_1-\boldsymbol{r}_2)$, one can rewrite the two-electron wavefunction amplitude in a separable form

$$P^{e} = \frac{P_0(\boldsymbol{r}_{10},\boldsymbol{r}_{20})}{J^{e}} = \frac{P_0(\boldsymbol{r}_{10},\boldsymbol{r}_{20})}{J_1^{e}J_2^{e}J_{12}^{e}}. \tag{71}$$

Here we introduced the auxiliary Jacobians

$$J_j^{e} = 1 - \int_T^t dt' \int_T^{t'} d\tau\, \Delta_1 U[\boldsymbol{r}_{jL}(\tau)], \tag{72}$$

$$J_{12}^{e} = 1 - 2\int_T^t dt' \int_T^{t'} d\tau\, \Delta_1 V^{ee}[\boldsymbol{r}_{12} + \Delta\boldsymbol{k}(\tau - t)]. \tag{73}$$

Similarly, one can also rewrite the adiabatic approximation to the amplitude Eq. (67) in separable form

$$P^{\mathrm{ad}}(\boldsymbol{r}_1,\boldsymbol{r}_2,t) = P_0(\boldsymbol{r}_{10},\boldsymbol{r}_{20})P_1P_2P_{12}, \tag{74}$$

$$P_1(\boldsymbol{r}_1,\boldsymbol{r}_2,t) = \left|1 + \frac{\boldsymbol{k}_{L1}(t)\boldsymbol{k}_{C1}(t)}{|\boldsymbol{k}_{L1}(t)|^2}\right|^{-1/2}, \tag{75}$$

$$P_2(\boldsymbol{r}_1,\boldsymbol{r}_2,t) = \left|1 + \frac{\boldsymbol{k}_{L2}(t)\boldsymbol{k}_{C2}(t)}{|\boldsymbol{k}_{L2}(t)|^2}\right|^{-1/2}, \tag{76}$$

$$P_{12}(\boldsymbol{r}_1,\boldsymbol{r}_2,t) = \left|1 + 2\frac{\Delta\boldsymbol{k}\cdot\boldsymbol{k}_{12}(t)}{|\Delta\boldsymbol{k}|^2}\right|^{-1/2}. \tag{77}$$

Finally, the initial amplitude in the eikonal approximation is obtained using the same method as in the one-electron case above. This yields

$$P_0(\boldsymbol{r}_{10},\boldsymbol{r}_{20}) = \left|1 - \frac{U(\boldsymbol{r}_{10})}{k_1^2} - \frac{U(\boldsymbol{r}_{20})}{k_2^2} - 2\frac{V^{ee}(\boldsymbol{r}_{10}-\boldsymbol{r}_{20})}{\Delta k_2^2}\right|^{-1/2}. \tag{78}$$

The initial amplitude can also be written in a separable form

$$P_0(\boldsymbol{r}_{10},\boldsymbol{r}_{20}) = P_{01}P_{02}P_{012}, \tag{79}$$

$$P_{01}(\boldsymbol{r}_{10}) = \left|1 - \frac{U(\boldsymbol{r}_{10})}{k_1^2}\right|^{-1/2}, \tag{80}$$

$$P_{02}(\boldsymbol{r}_{20}) = \left|1 - \frac{U(\boldsymbol{r}_{20})}{k_2^2}\right|^{-1/2}, \tag{81}$$

$$P_{012}(\boldsymbol{r}_{10},\boldsymbol{r}_{20}) = \left|1 - 2\frac{V^{ee}(\boldsymbol{r}_{10}-\boldsymbol{r}_{20})}{\Delta k_2^2}\right|^{-1/2}. \tag{82}$$

This derivation shows that the generalization to the case of n-interacting continuum electrons is straightforward. The advantage of this solution is that it includes the interaction with the binding potential and the interaction between the electrons at the same level of accuracy.

V. QUASIENERGY SOLUTIONS

The quasienergy method (for early papers, see, e.g., [60–63]) is often applied to the analysis of quantum systems with time-periodic Hamiltonians $\hat{H}(t+T_L)=\hat{H}(t)$. The quasienergy states (QES), $\psi_E(\boldsymbol{r},t)$, are solutions of the time dependent Schrödinger equation that have the specific form

$$\psi_E(\boldsymbol{r},t) = \phi_E(\boldsymbol{r},t)e^{-iEt}, \tag{83}$$

$$\phi_E(\boldsymbol{r},t+T_L) = \phi_E(\boldsymbol{r},t). \tag{84}$$

The quasienergy E is a real number and the functions $\phi_E(\boldsymbol{r},t)$ satisfy the equation

$$\left[\hat{H}(t) - i\frac{\partial}{\partial t}\right]\phi_E(\boldsymbol{r},t) = E\phi_E(\boldsymbol{r},t). \tag{85}$$

We now show that in the limit of long propagation times $|t-T|\to\infty$ (the modulus incorporates both the cases of forward and backward propagation) the eikonal-Volkov solutions derived above,

$$\Psi_{\boldsymbol{k},T}^{\mathrm{eV}} = \Psi_{\boldsymbol{k},T}^{V}(\boldsymbol{r},t)P^{e}(\boldsymbol{r},t)e^{iG_{\boldsymbol{k},T}(\boldsymbol{r},t)} \tag{86}$$

[see Eqs. (11), (15), and (41)], have the form of the QES with the quasienergy $E=k^2/2$. The superscript eV in solutions given by Eq. (86) stands for the eikonal-Volkov states. Extracting the quasienergy part from the eV states we introduce $\tilde{\phi}_E^{\mathrm{eV}}(\boldsymbol{r},t)$, an analog of the states $\phi_E(\boldsymbol{r},t)$ defined in Eq. (83)

$$\Psi_{\boldsymbol{k},T}^{\mathrm{eV}} = \tilde{\phi}_E^{\mathrm{eV}}(\boldsymbol{r},t)e^{-i(k^2/2)t}. \tag{87}$$

Now we shall prove that the states $\tilde{\phi}_E^{\mathrm{eV}}(\boldsymbol{r},t)$ satisfy Eq. (84) as $|t-T|\to\infty$. We begin by noting that for finite propagation times these states contain both the periodic and transient terms. The transient terms are $P_0(\boldsymbol{r}_0)$ in the amplitude and $G_{0\boldsymbol{k}}(\boldsymbol{r}_0)$ in the phase, where $\boldsymbol{r}_0$ depends on time; see Eq. (17). These terms are related to the turn-on of the interaction with the laser field.

The contribution of the transient terms to the states $\tilde{\phi}_E^{\mathrm{eV}}(\boldsymbol{r},t)$ decreases with increasing propagation time and disappears in the limit of very long propagation times $|t-T|\to\infty$. Indeed, for $|t-T|\to\infty$ the initial coordinate $\boldsymbol{r}_0\propto-\boldsymbol{k}(t-T)\to\pm\infty$. Substituting this result into Eq. (55) yields $P_0^{e}(\boldsymbol{r}_0)\to 1$. Choosing the z axis along the direction of $\boldsymbol{k}$ one can rewrite Eqs. (23) and (24) as

$$G_{0\boldsymbol{k}}^{(\pm)}(x,y,z) = \mp\frac{1}{k}\int_{z_0}^{\mp\infty} dz'\, U(x,y,z'). \tag{88}$$

In the limit $|t-T|\to\infty$ we obtain $z_0\to-\infty$ for $G_{0\boldsymbol{k}}^{(+)}$ and $z_0\to+\infty$ for $G_{0\boldsymbol{k}}^{(-)}$, yielding $G_{0\boldsymbol{k}}^{(\pm)}(\boldsymbol{r}_0)\to 0$.

Let us show that the remaining terms in $\tilde{\phi}_E^{\mathrm{eV}}(\boldsymbol{r},t)$

$$G_{\boldsymbol{k},T}^{\omega}(\boldsymbol{r},t) \equiv -\int_T^t U(\boldsymbol{r}_L(\tau))d\tau, \tag{89}$$

$$P^{\omega}(\boldsymbol{r},t) \equiv \left|1-\int_T^t dt' \int_T^{t'} d\tau\, \Delta U[\boldsymbol{r}_L(\tau)]\right|^{-1/2} \tag{90}$$

are indeed periodic in time in the limit $|t-T| \to \infty$.

If the function $G_{\boldsymbol{k},T}^{\omega}(\boldsymbol{r},t)$ is periodic in time with the period T_L, then shifting the initial moment of time by one period should not change the solution. Therefore, the difference between the solutions $\Delta G^{\omega}=G_{\boldsymbol{k},nT_L}^{\omega}(\boldsymbol{r},t)-G_{\boldsymbol{k},(n-1)T_L}^{\omega}(\boldsymbol{r},t)$,

$$\Delta G^{\omega} \equiv \int_{(n-1)T}^{nT} U(\boldsymbol{r}_L(\tau))d\tau, \tag{91}$$

should tend to zero. Since the binding potential is a monotonic function of coordinates far from the origin, one obtains

$$U[\boldsymbol{r}_L(nT_L)] < \int_{(n-1)T}^{nT} U(\boldsymbol{r}_L(\tau))d\tau < U[\boldsymbol{r}_L((n-1)T_L)]. \tag{92}$$

In the limit of very long propagation times $n \to \infty$ both $U[\boldsymbol{r}_L((n-1)T_L)] \to 0$ and $U[\boldsymbol{r}_L(nT_L)] \to 0$, which proves that $\Delta G^{\omega} \to 0$. Analogously, one can prove the periodicity of $P^{\omega}(\boldsymbol{r},t)$, given by Eq. (90). The part of the solution $\tilde{\phi}_E^{\mathrm{eV}}(\boldsymbol{r},t)$ represented by the Volkov phase $S_V^{\omega}(\boldsymbol{r},t)=S_{\boldsymbol{k},T}^{V}(\boldsymbol{r},t)+(i/2)\int_T^t \boldsymbol{k}^2 d\tau$ is periodic in time for any moment of time t, if at this moment $\boldsymbol{A}(t)=\boldsymbol{A}(t+T_L)$. Therefore, the eV quasienergy solutions have the form given by Eq. (83) with $E=k^2/2$ and $\phi_E(\boldsymbol{r},t)=\phi_E^{\mathrm{eV}}(\boldsymbol{r},t)$, where

$$\phi_E^{\mathrm{eV}}(\boldsymbol{r},t) = \frac{1}{(2\pi)^{3/2}} P^{\omega}(\boldsymbol{r},t) e^{iS_V^{\omega}(\boldsymbol{r},t)+iG_{\boldsymbol{k},T}^{\omega}(\boldsymbol{r},t)}. \tag{93}$$

VI. APPLICATIONS TO STRONG-FIELD PROBLEMS

Sections VI and VII aim at developing the EVA approach. In this section we consider the application of the eikonal-Volkov (eV) solutions to different strong-field problems. Further in this section we shall use the following types of the solutions for regimes (A) and (C) (see Sec. II B):

$$\Psi_{\boldsymbol{k},T}^{\mathrm{eV}}(\boldsymbol{r},t) = \Psi_{\boldsymbol{k},T}^{V}(\boldsymbol{r},t) e^{iG_{\boldsymbol{k},T}(\boldsymbol{r},t)}, \tag{94}$$

$$\Psi_{\boldsymbol{k}_1,\boldsymbol{k}_2,T}^{\mathrm{eV}(2e)} = \Psi_{\boldsymbol{k}_1,T}^{\mathrm{eV}}(\boldsymbol{r}_1,t)\Psi_{\boldsymbol{k}_2,T}^{\mathrm{eV}}(\boldsymbol{r}_2,t) e^{iG_{12,\Delta\boldsymbol{k}}(\boldsymbol{r}_1,\boldsymbol{r}_2,t)}, \tag{95}$$

and for regime (B)

$$\Phi_{\boldsymbol{k},T}^{\mathrm{eV}}(\boldsymbol{r},t) = P_{\mathrm{WKB}}^{\mathrm{ad}}(\boldsymbol{r},t)\Psi_{\boldsymbol{k},T}^{V}(\boldsymbol{r},t) e^{i\sigma_{\boldsymbol{k},T}(\boldsymbol{r},t)}. \tag{96}$$

Here $\Psi_{\boldsymbol{k},T}^{V}(\boldsymbol{r},t)$ is Volkov function given by Eq. (11). The dynamics of strong field ionization, considered in Sec. VI B, can be attributed to regime (A). In strong-field ionization, direct electrons are born away from the core with low momenta and never return back to pass the core. The regularization procedure is not required here and we use the first class of solutions, Eq. (94), with nonregularized phase $G_{\boldsymbol{k},T}(\boldsymbol{r},t)$ [Eq. (15)].

The dynamics of the electrons produced via one-photon XUV ionization in the strong laser field, considered in Sec. VI D, belongs to regime (B). In this case the characteristic trajectory starts near the core, the electron has high momentum and rapidly moves away from the core. In this case we use the second class of solutions given by Eq. (96), with the regularized phase $\sigma_{\boldsymbol{k},T}(\boldsymbol{r},t)$ [Eq. (30)] and the adiabatic amplitude $P_{\mathrm{WKB}}^{\mathrm{ad}}(\boldsymbol{r},t)$ [Eq. (51)].

The electron dynamics leading to high-energy above threshold ionization (ATI) and non-sequential double ionization (NSDI) belongs to regime (C). The recollision electrons can have both low and high energies. While the correct description of the low-energy recollision electrons may not be important for ATI, since in the final spectra these electrons are typically buried under the direct electrons, it is important for NSDI, which does not look at the direct electrons. The eikonal-Volkov solutions can not be used directly to describe the recollision dynamics, since they can not describe hard collisions.

In Sec. VI C we will show how to describe dynamics in regime (C) using the appropriate partitioning procedure in the strong-field S-matrix formalism. This partitioning has a builtin regularization procedure that follows from the post-form of S-matrix expression for ATI and NSDI and uses one-electron and two-electron solutions given by Eqs. (94) and (95).

We begin the discussion with another partitioning formalism, known as Adams' partitioning [64], which we use as the first step in applying the eikonal-Volkov continuum solutions.

A. Adams' partitioning

Consider the one electron case. The generalization to two-electron case is given in Sec. VI C.

We formally define the eikonal-Volkov propagator $\hat{\mathcal{U}}(t,T)$ as

$$\Psi_{\boldsymbol{k},T}^{\mathrm{eV}}(\boldsymbol{r},t) \equiv \hat{\mathcal{U}}(t,T)\Psi_{\boldsymbol{k},T}^{\mathrm{eV}}(\boldsymbol{r},T), \tag{97}$$

$$\Psi_{\boldsymbol{k},T}^{\mathrm{eV}}(\boldsymbol{r},T) \equiv P_0^e(\boldsymbol{r}) e^{iG_{0\boldsymbol{k}}^{(\pm)}(\boldsymbol{r})}. \tag{98}$$

Here $G_{0\boldsymbol{k}}^{(\pm)}(\boldsymbol{r})$ is given by Eqs. (22) and (21) and $P_0^e(\boldsymbol{r})$ is given by Eq. (55). To develop the formal approach, which is conceptually different from the standard S-matrix approach, we divide the Hilbert space into two subspaces, Ω_1 and Ω_2. In the subspace Ω_2 the approximate propagator $\hat{\mathcal{U}}(t,T)$ is expected to be accurate, while in the subspace Ω_1 it is not. The idea is to apply the approximate propagator only to the subspace Ω_2 where it is expected to work. Formally, this can be achieved using the following partitioning procedure.

Let us define the projection operator $\hat{P}_1$ which selects the subspace Ω_1 of order s. For this operator we have $\hat{P}_1^2=\hat{P}_1$, $\hat{P}_1^{\dagger}=\hat{P}_1$, and $\mathrm{Tr}(\hat{P}_1)=s$. Let $\hat{P}_2=\hat{I}-\hat{P}_1$ be the projection operator, which selects the orthogonal subspace Ω_2. Here $\hat{I}$ is

the identity operator. The operator $\hat{P}_2$ satisfies similar relations: $\hat{P}_2^2=\hat{P}_2$, $\hat{P}_2^\dagger=\hat{P}_2$. Since the two subspaces are orthogonal, we have $\hat{P}_1\hat{P}_2=\hat{P}_2\hat{P}_1=0$. The finite dimensionality of the subspace Ω_1 is natural for describing strong field ionization, as discussed below.

Now the Hamiltonian $\hat{H}=\hat{H}_0+\hat{V}_L(t)$ includes four operators: (i) One acting only on the first subspace, (ii) one acting only on the second subspace, and (iii) two operators describing the coupling between the two subspaces

$$\hat{H}=\hat{H}_{11}+\hat{H}_{22}+[\hat{H}_{12}+\hat{H}_{21}], \tag{99}$$

$$\hat{H}_{ij}=\hat{P}_i\hat{H}\hat{P}_j, \quad i,j=1,2. \tag{100}$$

The solution $|\Psi(t)\rangle$ of the Schrödinger equation

$$i\frac{\partial|\Psi(t)\rangle}{\partial t}=\hat{H}|\Psi(t)\rangle \tag{101}$$

now has two orthogonal components

$$|\Psi(t)\rangle=|\Psi_1(t)\rangle+|\Psi_2(t)\rangle, \tag{102a}$$

$$|\Psi_j(t)\rangle=\hat{P}_j|\Psi(t)\rangle, \quad j=1,2. \tag{102b}$$

Thus the wave vector is broken into two components and the Hamiltonian matrix into four blocks. This type of partitioning of the full Hamiltonian H into a zero-order Hamiltonian and the perturbation, given by the off-diagonal blocks was first suggested by Adams [64] for time-independent Hamiltonians in problems of quantum chemistry.

Using Eqs. (99)–(102), one obtains the equations for the wave-function components Ψ_1 and Ψ_2 in the orthogonal subspaces $(i,j=1,2,\ i\neq j)$

$$i\frac{\partial|\Psi_i(t)\rangle}{\partial t}=\hat{H}_{ii}|\Psi_i(t)\rangle+\hat{H}_{ij}|\Psi_j(t)\rangle. \tag{103}$$

Writing these differential equations in integral form with the initial condition $|\Psi_1(t_0)\rangle=|\Psi_1^{(0)}\rangle$, and $|\Psi_2(t_0)\rangle=0$, we obtain

$$|\Psi_2(t)\rangle=-i\int_{t_0}^{t}dt'\hat{\mathcal{T}}e^{-i\int_{t'}^{t}\hat{H}_{22}(\xi)d\xi}\hat{H}_{21}(t')|\Psi_1(t')\rangle, \tag{104}$$

$$|\Psi_1(t)\rangle=-i\int_{t_0}^{t}dt'\hat{\mathcal{T}}e^{-i\int_{t'}^{t}\hat{H}_{11}(\xi)d\xi}\hat{H}_{12}(t')|\Psi_2(t')\rangle + \hat{\mathcal{T}}e^{-i\int_{t_0}^{t}\hat{H}_{11}(\xi)d\xi}|\Psi_1^{(0)}\rangle. \tag{105}$$

Here $\hat{\mathcal{T}}$ is the time-ordering operator (see, e.g., [65]). From now on we omit $\hat{\mathcal{T}}$ for brevity in front of the exponents implying the evolution operators. We can now apply these exact equations to the specific problems, combining the formalism with the approximate eikonal-Volkov solutions.

B. EVA for subcycle dynamics of strong-field ionization

Strong field ionization has a rich dynamics on the subcycle time scale [66]. This dynamics has been recently observed in a pump-probe type experiment involving attosecond XUV pulses [67]. To set up the background for further discussion, Fig. 7 explicitly illustrates the inaccuracies of the SFA by showing the growth of the continuum population obtained using SFA [Fig. 7(a)] and numerical simulations [Fig. 7(b)]. Subcycle dynamics as predicted by SFA is wrong both qualitatively and quantitatively (see [17] for details).

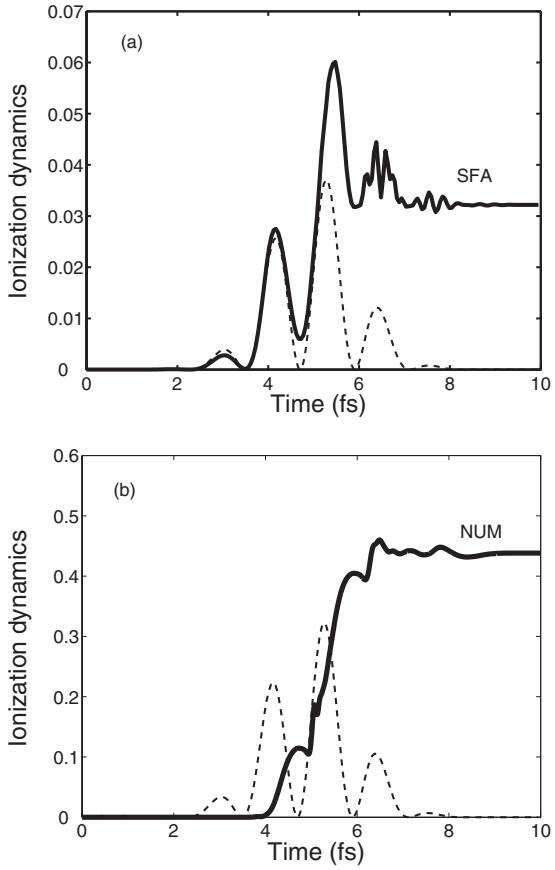

FIG. 7. Subcycle ionization dynamics (a) as predicted by SFA and (b) calculated numerically. For details, see [17]. Thin dashed line shows the laser field, with the wavelength $\lambda=800$ nm. The laser field amplitude is $\mathcal{E}_0=0.065$ a.u. (intensity $I=1.5\times10^{14}$ W/cm^2). The system is a 1D soft-core Coulomb potential with the ionization potential of Xe, $I_p=12.13$ eV.

To demonstrate the ability of eikonal-Volkov functions to restore both quantitative and qualitative picture of the subcycle ionization dynamics, we will apply the formalism developed above to this specific problem.

Since the eikonal-Volkov states treat the binding potential perturbatively, the corresponding propagator has to be restricted to a subspace of the full Hilbert space, where perturbative treatment is appropriate. Thus application of the eikonal-Volkov states should be combined with the Adams' partitioning procedure described above. The eikonal-Volkov propagator is well-suited for this procedure since it keeps continuum states in the continuum.

Consider strong field ionization near the barrier suppression intensity. In this case the first subspace Ω_1 will include only one state—the ground state $|g\rangle$. All other bound and continuum states $|k\rangle$ are assigned to the second sub-space Ω_2.

Indeed, in the vicinity of barrier suppression intensities all excited states of the field-free system are embedded into the continuum and therefore the strong laser field dominates their dynamics.

Thus the relevant projection operators are defined as follows: $\hat{P}_1=|g\rangle\langle g|$, $\hat{P}_2=\hat{I}-|g\rangle\langle g|$, and the wave vector $|\Psi_1(t)\rangle \equiv \hat{P}_1|\Psi(t)\rangle$ becomes

$$|\Psi_1(t)\rangle = |g\rangle\langle g|\Psi(t)\rangle = a_g(t)e^{-iE_g(t-t_0)}|g\rangle. \tag{106}$$

The amplitudes $c(\boldsymbol{k},T)$ determine the photoelectron spectrum and ionization yield after the end of the laser pulse $t=T$, where $|\boldsymbol{k}\rangle$ denotes continuum state with asymptotic momentum $\boldsymbol{k}$

$$c(\boldsymbol{k},T) \equiv \langle \boldsymbol{k}|P_2\Psi(T)\rangle. \tag{107}$$

Then, we use Eq. (104) and the identity $\hat{H}_{21}=\hat{P}_2\hat{V}_L\hat{P}_1$ to obtain

$$c(\boldsymbol{k},T) = -i\int_{t_0}^{T} dt'\langle \boldsymbol{k}|e^{-i\int_{t'}^{T}\hat{H}_{22}(\xi)d\xi}\hat{P}_2\hat{V}_L(t')\hat{P}_1|g\rangle \times a_g(t')e^{-iE_g(t'-t_0)}. \tag{108}$$

The use of truncated propagators that keep the dynamics confined to a subspace orthogonal to the subspace containing the initially populated state allows us to introduce a measure of the *subcycle* ionization dynamics. First, we introduce the field-dressed states

$$\langle \boldsymbol{k}|e^{-i\int_{t}^{T}\hat{H}_{22}(\xi)d\xi} \equiv \langle \boldsymbol{k}|\hat{\mathcal{U}}_{22}(T,t) \equiv \langle \boldsymbol{k}(t)|. \tag{109}$$

These states $\langle \boldsymbol{k}(t)|$ are constructed by back-propagation of the field-free continuum states defined at the end of the pulse T. In contrast to $|\Psi_2(t)\rangle$, which is "pumped" from the first subspace, the evolution governed by $\hat{\mathcal{U}}_{22}(T,t)$ is confined to the second subspace. The states $|\boldsymbol{k}(t)\rangle$ remain orthogonal to $|g\rangle$ and are unaffected by the population transfer between the subspaces 1 and 2. Therefore, the dressed states $|\boldsymbol{k}(t)\rangle$ present a convenient basis for calculating the ionization dynamics. We now introduce the amplitude for populating these states at time t

$$c_{\boldsymbol{k},T}(t) = \langle \boldsymbol{k}(t)|\Psi_2(t)\rangle = -i\int_{t_0}^{t} dt'\langle \boldsymbol{k}|e^{-i\int_{t'}^{T}\hat{H}_{22}(\xi)d\xi} \times \hat{V}_L(t')a_g(t')|g\rangle e^{-iE_g(t'-t_0)}. \tag{110}$$

As can be seen by comparing Eq. (110) with Eq. (108), this results in keeping T in the upper limit of the final state propagator while using the instantaneous time t in the upper limit of the integral over t'. Note that the $|\boldsymbol{k}(t)\rangle$ remain orthogonal to each other during the whole unitary evolution. The subcycle ionization yield is then defined as

$$W_T(t) \equiv \int d\boldsymbol{k}|c_{\boldsymbol{k},T}(t)|^2. \tag{111}$$

The physical idea behind this definition is to use the basis that is more appropriate in the presence of the strong laser field, when the field-free basis loses its physical meaning. At the same time, the dressed basis turns into the field-free basis when the laser is turned off.

The ionization yield is dominated by the direct electrons. These electrons never come back to recollide with the core. Therefore we approximate the truncated propagator $\langle \boldsymbol{k}|e^{-i\int_{t'}^{T}\hat{H}_{22}(\xi)d\xi}$ with the eikonal-Volkov propagator [Eq. (97)] (for details, see Ref. [17])

$$\langle \boldsymbol{k}^e|\hat{\mathcal{U}}(T,t) \equiv \langle \boldsymbol{k}^{\mathrm{eV}}(t)|, \tag{112}$$

$$\langle \boldsymbol{k}^e|\boldsymbol{r}\rangle = P_0^e(\boldsymbol{r})e^{-iG_{0\boldsymbol{k}}^{(-)}(\boldsymbol{r})}, \tag{113}$$

$$\langle \boldsymbol{k}^{\mathrm{eV}}(t)|\boldsymbol{r}\rangle = \Psi_{\boldsymbol{k},T}^{*\mathrm{eV}}(\boldsymbol{r},t). \tag{114}$$

Here $G_{0\boldsymbol{k}}^{(\pm)}(\boldsymbol{r})$ is given by Eqs. (22) and (21), $P_0^e(\boldsymbol{r})$ is given by Eq. (55), and $\Psi_{\boldsymbol{k},T}^{\mathrm{eV}}(\boldsymbol{r},t)$ is given by Eq. (94). Note that here T is the final moment of time after turnoff of the laser field. The procedure of Eq. (112) implies back propagation of field-free eikonal states $\langle \boldsymbol{k}^e|$, corresponding to the incoming-type solution [Eq. (21)]. This procedure yields

$$c_{\boldsymbol{k},T}^{\mathrm{eV}}(t) = \langle \boldsymbol{k}^{\mathrm{eV}}(t)|\Psi_2^{(0)}(t)\rangle = -i\int_{t_0}^{t} dt'\langle \boldsymbol{k}^{\mathrm{eV}}(t')|\hat{V}_L(t')a_g(t')e^{-iE_g(t'-t_0)}|g\rangle, \tag{115a}$$

$$W_T^{\mathrm{eV}}(t) \equiv \int d\boldsymbol{k}|c_{\boldsymbol{k},T}^{\mathrm{eV}}(t)|^2. \tag{115b}$$

Here $|\Psi_2^{(0)}(t)\rangle$, given by

$$|\Psi_2^{(0)}(t)\rangle = -i\int_{t_0}^{t} dt'\hat{\mathcal{U}}(t,t')\hat{V}_L(t')a_g(t')e^{-iE_g(t'-t_0)}|g\rangle, \tag{116}$$

is the zeroth-order approximation to $|\Psi_2(t)\rangle$ with respect to electron collisions with the core, describing the dynamics of direct electrons. The next-order approximation, corresponding to one hard recollision, will be considered in the next section.

A comparison of the results of direct numerical simulations with the results obtained by calculating the integrals Eqs. (115a) and (115b) [Fig. 8(a)] for the 1D model described above are in agreement up to about 10–15 % not only for the total ionization yields, but also for the subcycle dynamics of the strong-field ionization. For the details of numerical procedure, see Ref. [17].

Figure 8(b) shows the subcycle ionization yield calculated using the adiabatic approximation Eq. (33) for the phase of the eikonal-Volkov functions in Eq. (115a). As expected, this additional approximation degrades the agreement with the numerical results. The "steps" are not proportional to the maximal strength of the field on each half cycle and the "dips" characteristic for short-range potentials with a single state (see [17]) are no longer compensated.

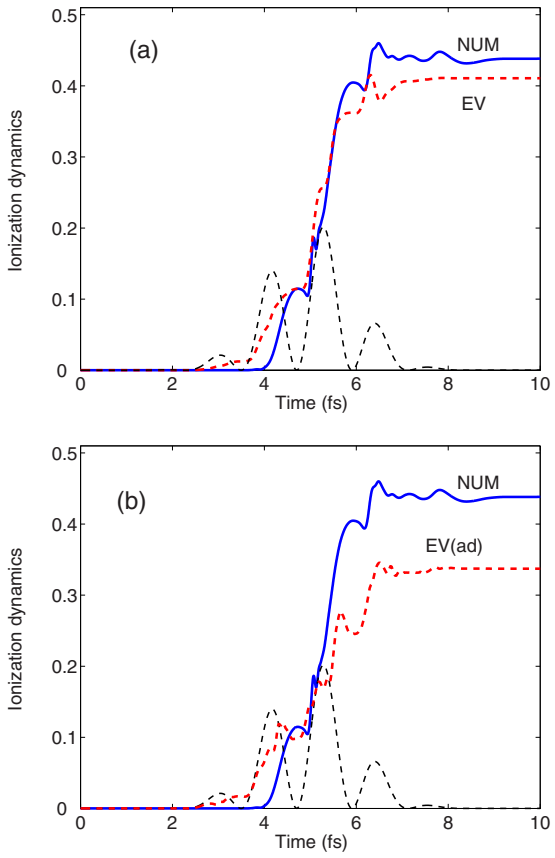

FIG. 8. (Color online) Subcycle ionization dynamics around the barrier suppression field. Solid line shows results of numerical simulation and dashed line shows $W_T(t)$ (a) obtained with the eikonal-Volkov solutions and (b) obtained with the adiabatic approximation to the eikonal-Volkov solutions. Thin dashed line shows the laser pulse, with $\lambda=800$ nm. The laser field amplitude is $\mathcal{E}_0=0.065$ a.u. ($I=1.5\times10^{14}$ W/cm^2); the model system is the 1D soft-core Coulomb potential with $I_p=12.13$ eV.

C. EVA for elastic and inelastic recollision

Electron recollision [68] lies at the core of essentially all strong field phenomena in the infrared range of frequencies. In this process, an electron liberated during strong field ionization near the peak of the laser field oscillation is first driven by the laser field away from the core. During the next half cycle, when the electric field of the laser changes direction, the field can reverse the momentum of the electron and force it to recollide with the parent ion. Elastic recollision leads to the generation of "hot" ATI electrons [1,2,69]—electrons with energies up to $10U_p$. Inelastic recollision is a dominant channel underlying nonsequential double ionization (NSDI) [4] in infrared fields [38].

In this section we show how eV functions can be used to describe the electron spectra of ATI and NSDI. Since both processes involve electron recollision hard collisions have to be treated explicitly.

1. Above-threshold ionization: Direct and high-energy electrons

To describe hard collision, we use the "post" version of the S-matrix formalism (see, e.g., [38,70]). We formally partition the Hamiltonian as $\hat{H}=\hat{H}_f+\hat{V}_f$. The potential $\hat{V}_f$, responsible for the hard collision with the core, will be defined below. The solution $|\Psi(t)\rangle$ of the time dependent Schrödinger equation is

$$|\Psi(t)\rangle = -i\int_{t_0}^{t} dt' e^{-i\int_{t'}^{t}\hat{H}_f(\xi)d\xi}\hat{V}_f(t')|\Psi(t')\rangle + e^{-i\int_{t_0}^{t}\hat{H}_f(\xi)d\xi}|g\rangle. \tag{117}$$

Expanding the solution in powers of V_f, $|\Psi(t)\rangle=|\Psi^{(0)}(t)\rangle+|\Psi^{(1)}(t)\rangle+\cdots$, and using Eqs. (102), for the continuum part of $|\Psi(t)\rangle$ we obtain

$$\begin{aligned}|\Psi_2(t)\rangle &= P_2|\Psi(t)\rangle \\ &\simeq |\Psi_2^{(0)}(t)\rangle + |\Psi_2^{(1)}(t)\rangle \\ &\simeq |\Psi_2^{(0)}(t)\rangle - i\int_{t_0}^{t} dt' e^{-i\int_{t'}^{t}\hat{H}_f(\xi)d\xi}\hat{V}_f(t')|\Psi_2^{(0)}(t')\rangle.\end{aligned} \tag{118}$$

Here $|\Psi_2^{(0)}(t)\rangle$ describes the direct electrons and is given by Eq. (116) in the previous section.

Let us now take a closer look at the structure of the Hamiltonian $\hat{H}=\hat{H}_f+\hat{V}_f$. To model electron scattering on the parent atomic or molecular ion one can introduce an effective potential given by three main components: Electrostatic potential, exchange potential, and polarization potential. The electrostatic potential consists of the Coulomb potential of the nuclei and the Hartree potential of the bound electrons. The nonlocal exchange potential can be reduced to or replaced with the local potential [71–74]. In Refs. [75,76] it was shown that nonlocal contributions can be partially included through a suitable modification of matrix elements. Finally, the polarization potential, describing the polarization of the parent ion by the continuum electron is proportional to α/r^4, where α is the polarizability of the ion core.

The total potential constructed as described above can now be split into two parts: The short-range singular part and the long-range nonsingular part. The short-range part includes exchange V^{ex}, polarization V^{pol}, and the short-range singular part of the electrostatic potential $V^{\text{el}}_{\text{short}}$. The nonsingular part describes the long-range electrostatic potential $V^{\text{el}}_{\text{long}}$.

To split the electrostatic potential into two parts, one needs an auxiliary short-range function $F(\boldsymbol{r})$, such that $V^{\text{el}}_{\text{sh}}(\boldsymbol{r})=F(\boldsymbol{r})\cdot V^{\text{el}}(\boldsymbol{r})$ and $V^{\text{el}}_{\text{long}}(\boldsymbol{r})=[1-F(\boldsymbol{r})]\cdot V^{\text{el}}(\boldsymbol{r})$; see, e.g., the standard techniques for splitting the Coulomb operator [77,78]. Note that if Eq. (117) is solved exactly, the choice of the auxiliary short-range function $F(\boldsymbol{r})$ does not change the result. Once approximations are made, the result may depend on $F(\boldsymbol{r})$.

Let us now combine this partitioning with the eikonal approximation applied to the long-range, nonsingular part of the interaction potential $V^{\text{el}}_{\text{long}}(\boldsymbol{r})$. By choosing the function $F(\boldsymbol{r})$, one can filter out the part of $V^{\text{el}}(\boldsymbol{r})$ which will not be described well in the eikonal approximation, for characteris-

tic continuum electron energies. As long as the eikonal approximation works for $V_{\text{long}}^{\text{el}}(\boldsymbol{r})$, the result will be insensitive to $F(\boldsymbol{r})$.

Now we determine the partitioning procedure as follows:

$$\hat{H}_f = \hat{\boldsymbol{p}}^2/2 + V_{\text{long}}^{\text{el}}(\boldsymbol{r}) + \hat{V}_L \equiv \hat{H}_{\text{reg}}, \tag{119}$$

$$\hat{V}_f = V^{\text{ex}}(\boldsymbol{r}) + V^{\text{pol}}(\boldsymbol{r}) + V_{\text{sh}}^{\text{el}}(\boldsymbol{r}) \equiv \hat{V}_{\text{sh}}. \tag{120}$$

The Hamiltonian $\hat{H}_f$ introduced above describes motion in the regularized potential $V_{\text{long}}^{\text{el}}(\boldsymbol{r})$, which does not have a singularity by definition. This regularization favors the application of eikonal-Volkov functions given by Eq. (94) with $U(\boldsymbol{r}) = V_{\text{long}}^{\text{el}}(\boldsymbol{r})$. For such functions we also use the notation $\langle \boldsymbol{r} | \boldsymbol{k}_{\text{reg}}^{\text{eV}}(t) \rangle$. Then, the population amplitudes of the continuum states are

$$\begin{aligned} b^{\text{eV}}(\boldsymbol{k},T) &\equiv \langle \boldsymbol{k}^e | P_2 | \Psi(t) \rangle \\ &= c_{\boldsymbol{k},T}^{\text{eV}}(T) - i\int_{t_0}^{T} dt' \langle \boldsymbol{k}_{\text{reg}}^{\text{eV}}(t') | \hat{V}_{\text{sh}} | \Psi_2^{(0)}(t') \rangle \\ &= c_{\boldsymbol{k},T}^{\text{eV}}(T) - i\int_{t_0}^{T} dt' \int d\boldsymbol{p} \langle \boldsymbol{k}_{\text{reg}}^{\text{eV}}(t') | \hat{V}_{\text{sh}} | \boldsymbol{p}^{\text{eV}}(t') \rangle c_{\boldsymbol{p},T}^{\text{eV}}(t'). \end{aligned} \tag{121}$$

Here T is chosen as the moment of observation after the turnoff of the laser field and $c_{\boldsymbol{k},T}^{\text{eV}}(t) \equiv \langle \boldsymbol{k}^{\text{eV}}(t) | \Psi_2(t) \rangle$ is the population amplitudes due to "direct" electrons given by Eq. (115a). The integral term in Eq. (121) describes hot ATI electrons emerging due to the recollision process.

The above result is reminiscent of the treatment of hot ATI electrons within the improved SFA [69], with several key differences. First, our result includes multiple "soft" scattering events in the field of the long-range nonsingular potential $V_{\text{long}}(\boldsymbol{r})$, as opposed to the SFA treatment where the effect of the ion potential is neglected. Second, the partitioning procedure dictates that hard collision is described by the short-range potential. Therefore, the recollision process is described as a combination of a hard collision with the short range potential and subsequent evolution in the long-range nonsingular potential treated in the eikonal approximation.

2. Nonsequential double ionization

We can now consider the case of the two-electron continuum using the two-electron continuum wave functions, Eq. (95), which includes the electron-electron interaction and the interaction of the electrons with the binding potential.

For simplicity, we shall consider a two electron system. The Hamiltonian is

$$\hat{H}^{2e} = \sum_{j=1,2} [\hat{\boldsymbol{p}}_j^2/2 + U(\boldsymbol{r}_j) + \hat{V}_L(\boldsymbol{r}_j,t)] + V^{ee}(\boldsymbol{r}_{12}),$$

$$\boldsymbol{r}_{12} = \boldsymbol{r}_1 - \boldsymbol{r}_2, \tag{122}$$

where $U(\boldsymbol{r})$ is the attractive Coulomb potential of the core, $V^{ee}(\boldsymbol{r}_{12})$ describes the electron-electron interaction, and $\hat{V}_L$ describes the interaction of both electrons with the laser field.

The application of our formalism to NSDI starts with Eqs. (117) and (118). We have to (i) generalize Eq. (117) to the two-electron case and (ii) develop the appropriate partitioning procedure to introduce nonsingular potentials favorable for the eikonal approximation. We first specify the partitioning procedure and then consider the generalization of $|\Psi_2(t)\rangle$.

Using an auxiliary short-range function $F(\boldsymbol{r})$ as described above, we specify the partitioning procedure

$$\hat{H}_f = \sum_{j=1,2} [\hat{\boldsymbol{p}}_j^2/2 + V_{\text{long}}(\boldsymbol{r}_j) + \hat{V}_L(\boldsymbol{r}_j,t)] + V_{\text{long}}^{ee}(\boldsymbol{r}_{12}), \tag{123}$$

$$\hat{V}_f = V_{\text{sh}}(\boldsymbol{r}_1) + V_{\text{sh}}(\boldsymbol{r}_2) + V_{\text{sh}}(\boldsymbol{r}_{12}) = \hat{V}_{\text{coll}}. \tag{124}$$

The Hamiltonian $\hat{H}_f \equiv \hat{H}_{\text{reg}}$ [Eq. (123)] describes the motion in the regularized potential

$$U_{2e}^{\text{reg}} = V_{\text{long}}(\boldsymbol{r}_1) + V_{\text{long}}(\boldsymbol{r}_2) + V_{\text{long}}^{ee}(\boldsymbol{r}_{12}), \tag{125}$$

$$V_{\text{long}}(\boldsymbol{r}) \equiv U(\boldsymbol{r}) \cdot [1 - F(\boldsymbol{r})], \quad F(0) = 1, \tag{126}$$

$$V_{\text{long}}^{ee}(\boldsymbol{r}_{12}) \equiv V^{ee}(\boldsymbol{r}_{12}) \cdot [1 - F(\boldsymbol{r}_{12})]. \tag{127}$$

Such potential does not have the singularity and therefore the two-electron eikonal-Volkov functions should be accurate.

Before we consider the generalization of $|\Psi_2(t)\rangle$ from Eq. (118) for the two-electron case, we introduce the quasistatic dressed states of the ion $|n^+(t')\rangle$

$$\hat{H}^{1e} |n^+(t)\rangle = E_n^+(t) |n^+(t)\rangle, \tag{128}$$

$$\hat{H}^{1e} = \boldsymbol{p}^2/2 + U(\boldsymbol{r}) + \hat{V}_L(\boldsymbol{r},t). \tag{129}$$

Here the time dependence of the Hamiltonian is treated parametrically. In the intensity range where NSDI dominates double ionization, such an approximation should be sufficient for describing the evolution of the lowest ionic states in the low-frequency laser field.

We begin with the direct electrons. The formal generalization of the one-electron formalism requires projection operators $\hat{P}_1$ and $\hat{P}_2$ acting in the two-electron Hilbert space. For typical intensities where single ionization is significant, $\hat{P}_1 = |g\rangle\rangle\langle\langle g|$, where $|g\rangle\rangle$ is the ground state of the two-electron atom. (Here and below the double ket notation stresses the two-electron nature of the state.) This choice yields for the direct electrons produced by single ionization $|\Psi_2^{(0)}(t)\rangle\rangle$

$$|\Psi_2^{(0)}(t)\rangle\rangle = -i\int_{t_0}^{t} dt' e^{-i\int_{t'}^{t} \hat{H}_{22}^{2e}(\xi)d\xi} \hat{H}_{21}^{2e}(t') a_g(t') |g\rangle\rangle. \tag{130}$$

Here a_g is the projection of the total two-electron solution $|\Psi(t)\rangle\rangle$ on the two-electron ground state $a_g = \langle\langle g | \Psi(t)\rangle\rangle$, $\hat{H}_{21}^{2e} = \hat{P}_2 \hat{H}^{2e} \hat{P}_1 = \hat{V}_L(\boldsymbol{r}_1,t) + \hat{V}_L(\boldsymbol{r}_2,t)$. Now, unlike in the one-electron case, the propagator involving $\hat{H}_{22}$ acts on both elec-

trons: One is in the continuum; another remains bound in the ion. To stress this fact and calculate the propagator, we insert the resolution of identity for the one-electron continuum of the two-electron system after t'

$$\mathbb{I} = \sum |\boldsymbol{p}, n^+\rangle\langle \boldsymbol{p}, n^+|. \tag{131}$$

Here the basis vectors are symmetrized

$$|\boldsymbol{p}, n^+\rangle \equiv \hat{S}|\boldsymbol{p}^{\mathrm{eV}}(t)\rangle|n^+(t)\rangle \equiv \frac{1}{\sqrt{2}}[|\boldsymbol{p}^{\mathrm{eV}}\rangle|n^+\rangle + |n^+\rangle|\boldsymbol{p}^{\mathrm{eV}}\rangle] \tag{132}$$

as is appropriate for electrons with opposite spin. We rewrite $|\Psi_2^{(0)}(t)\rangle\rangle$ for the direct electrons as

$$|\Psi_2^{(0)}(t)\rangle\rangle = -i\int_{t_0}^{t} dt' e^{-i\int_{t'}^{t}\hat{H}_{22}^{2e}(\xi)d\xi}|\boldsymbol{p}, n^+\rangle\langle \boldsymbol{p}, n^+|\hat{V}_L(t')|g\rangle\rangle a_g(t'). \tag{133}$$

We can now discuss the matrix element at the moment t' and the propagator from t' to t. Consider first the matrix element $\langle \boldsymbol{p}, n^+|V_L(t')|g\rangle\rangle = E_L(t')\langle \boldsymbol{p}, n^+|\boldsymbol{r}_1 + \boldsymbol{r}_2|g\rangle\rangle$ from Eq. (133). The analysis follows [75].

The main component of this matrix element can be understood as the amplitude of transition from the Dyson orbital [79] defined as $|D_n(t)\rangle = \sqrt{2}\langle n^+(t)|g\rangle\rangle$ to the eikonal-Volkov continuum states $\langle \boldsymbol{p}^{\mathrm{eV}}(t)|\boldsymbol{r}|D_n(t)\rangle$. The second component of this matrix element describes the process where the laser field acts on the first electron, but liberates the second electron $\langle \boldsymbol{p}^{\mathrm{eV}}(t)|\widetilde{D}_n(t)\rangle$, where $|\widetilde{D}_n(t)\rangle = \sqrt{2}\langle n^+(t)|\boldsymbol{r}|g\rangle\rangle$. This exchange process is possible due to electron correlations in the ground state of the two electron atom. It is usually relatively weak compared to the direct process and will only affect the preexponential factor.

As a side note, for the plane wave continuum, the matrix element corresponding to the exchange process during ionization remains nonzero even in the absence of correlations. This artifact is largely avoided for the eV continuum functions, which include the effects of the core potential. We shall neglect the exchange process further on.

Now we consider the propagator $e^{-i\int_{t'}^{t}\hat{H}_{22}^{2e}(\xi)d\xi}|\boldsymbol{p}, n^+\rangle$ in Eq. (133). After strong field ionization the ion is most likely to be left in the ground quasistatic state $|g^+\rangle$. We will consider only this ionization channel, neglecting the shakeup during tunneling. Equation (132) yields

$$e^{-i\int_{t'}^{t}\hat{H}_{22}^{2e}(\xi)d\xi}|\boldsymbol{p}, g^+\rangle \simeq \frac{1}{\sqrt{2}}e^{-i\int_{t'}^{t}\hat{H}_{22}^{2e}(\xi)d\xi}|\boldsymbol{p}^{\mathrm{eV}}\rangle|g^+\rangle + \frac{1}{\sqrt{2}}e^{-i\int_{t'}^{t}\hat{H}_{22}^{2e}(\xi)d\xi}|g^+\rangle|\boldsymbol{p}^{\mathrm{eV}}\rangle. \tag{134}$$

We approximate Eq. (134) as follows:

$$e^{-i\int_{t'}^{t}\hat{H}_{22}^{2e}(\xi)d\xi}|\boldsymbol{p}^{\mathrm{eV}}\rangle|g^+(t')\rangle = |\boldsymbol{p}^{\mathrm{eV}}(t)\rangle|g^+(t)\rangle, \tag{135}$$

$$e^{-i\int_{t'}^{t}\hat{H}_{22}^{2e}(\xi)d\xi}|g^+(t')\rangle|\boldsymbol{p}^{\mathrm{eV}}\rangle = |g^+(t)\rangle|\boldsymbol{p}^{\mathrm{eV}}(t)\rangle. \tag{136}$$

The eikonal-Volkov functions are calculated using the Hamiltonian which includes the Coulomb potential of interaction with the core $U(\boldsymbol{r})$ and the Hartree potential $V^{\mathrm{SF}}(\boldsymbol{r},t)$

$$\hat{H}^{\mathrm{SF}} = \hat{\boldsymbol{p}}^2/2 + U(\boldsymbol{r}) + \hat{V}_L(\boldsymbol{r},t) + V^{\mathrm{SF}}(\boldsymbol{r},t), \tag{137}$$

$$V^{\mathrm{SF}}(\boldsymbol{r},t) = \langle g^+(t)|V^{ee}|g^+(t)\rangle. \tag{138}$$

We can now write the expression for the continuum amplitudes of the direct electrons

$$c_{\boldsymbol{p},T}^{\mathrm{eV}2e}(t) = -i\int_{t_0}^{t} dt' E_L(t')a_g(t')e^{-iE_g(t'-t_0)}\langle \boldsymbol{p}^{\mathrm{eV}}(t')|\boldsymbol{r}|D_g(t')\rangle\rangle, \tag{139}$$

where $D_g(t)$ is the Dyson orbital calculated using the quasistatic ground state of the ion.

Based on Eq. (139) we can write the expression for the two-electron spectrum

$$S = \frac{1}{2}|a^{\mathrm{eV}}(\boldsymbol{k}_1,\boldsymbol{k}_2) + a^{\mathrm{eV}}(\boldsymbol{k}_2,\boldsymbol{k}_1)|^2, \tag{140}$$

where

$$a^{\mathrm{eV}}(\boldsymbol{k}_1,\boldsymbol{k}_2) = -i\int_{t_0}^{T} dt' \int d\boldsymbol{p} \times \langle\langle \boldsymbol{k}_{\mathrm{reg}}^{2e}(t')|\hat{V}_{\mathrm{coll}}|\boldsymbol{p}^{\mathrm{eV}}(t')\rangle|g^+\rangle c_{\boldsymbol{p},T}^{\mathrm{eV}2e}(t'). \tag{141}$$

Similarly to the case of the elastic recollision considered above, the inelastic recollision is described here as a hard collision with a short range potential given by Eq. (124) and subsequent evolution in the laser field and in the nonsingular regularized potential Eq. (125), which can be treated in the eikonal approximation. The corresponding continuum functions $\langle\langle \boldsymbol{r}_1,\boldsymbol{r}_2|\boldsymbol{k}_{\mathrm{reg}}^{2e}(t)\rangle\rangle$ are given by Eq. (95) with $U(\boldsymbol{r}) = V_{\mathrm{long}}^{\mathrm{el}}(\boldsymbol{r})$ and $V^{ee}(\boldsymbol{r}) = V_{\mathrm{long}}^{ee}(\boldsymbol{r})$.

We see that in the presence of a strong laser field the effective potential responsible for the inelastic collision is short range. The long-range parts of the Coulomb interactions between the two electrons and with the core are incorporated into the eikonal Volkov functions, with the main effect being the addition of the eikonal phase to the Volkov phase. If one were to neglect the eikonal contribution to the phase, one would have arrived to the transitions between the Volkov states due to the scattering on the short-range potential, similar to the model investigated in detail in Ref. [80]. In that work, application of the short-range scattering potential was found to be superior to using the long-range scattering Coulomb potential in describing the experimental results on NSDI.

Figure 9 schematically shows the approximations we have made in this subsection. To calculate the lowest (second) order diagram describing NSDI [38] we use (i) the Hamiltonian $\hat{H}^{\mathrm{SF}}$ defined by Eq. (135) and the corresponding eV functions Eq. (94) for the continuum electron from the mo-

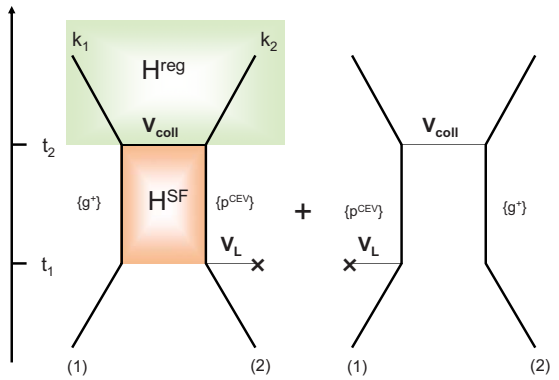

FIG. 9. (Color online) Second (lowest) order diagram for NSDI; see [38]. Two diagrams describe equivalent processes ensuring symmetry with respect to the two electrons. The approximations are schematically shown only in the left diagram. We use the Hamiltonian H^{SF} from Eq. (137) from the moment of ionization t_1 to the moment of recollision t_2 (red shaded area) and the regularized Hamiltonian equation (123) to describe the continuum motion of both liberated electrons from t_2 to the moment of observation T (green shaded area).

ment of ionization t_1 to the moment of recollison t_2 and (ii) the regularized Hamiltonian Eq. (123) and the corresponding two-electron eV functions Eq. (95) to describe the continuum motion of both liberated electrons from t_2 to the moment of observation T.

D. EVA for strong-field assisted XUV ionization

Laser assisted XUV ionization has become an important tool for characterizing modern few-cycle phase stabilized pulses and subfemtosecond XUV pulses. An XUV pulse initiates one-photon ionization at different phases of the IR laser field. Characterization procedures [81,82] exploit the photoelectron spectra recorded for different delays between the IR and XUV pulses.

Note also the deep connection between laser assisted XUV ionization and high harmonic generation (HHG) in strong laser fields: the emission of a high harmonic photon during the recombination to the initial state is inverse to the absorption of an XUV photon from this state. This connection allows one to use laser-assisted XUV absorption to address problems relevant for high harmonic generation, such as the influence of the ionic potential on HHG.

The full Hamiltonian of the problem is $\hat{H}_f = \hat{H}_0 + \hat{V}_L(t) + \hat{V}_X(t-t_X)$. Here $\hat{H}_0$ is the field-free Hamiltonian, $\hat{H} = \hat{H}_0 + \hat{V}_L(t)$ includes the interaction with the laser field but does not include the interaction with the XUV field. The interaction with the XUV pulse centered at t_X is described by $\hat{V}_X(t-t_X) = \boldsymbol{r}\vec{\mathcal{E}}_X(t-t_X)\exp(-i\Omega t)$, where $\mathcal{E}_X(t-t_X)$ is the electric field envelope and Ω is the carrier frequency.

Consider XUV pulses of low intensities initiating only one-photon processes. Then, the final state amplitude to find the electron with momentum $\boldsymbol{q}$ after the absorption of one XUV photon can be written as

$$c_X(\boldsymbol{q},t_X) = -i\int_{t_0}^{T} dt \langle \boldsymbol{q}|e^{-i\int_t^T \hat{H}(\xi)d\xi}\hat{V}_X(t-t_X)e^{-i\int_{t_0}^{t}\hat{H}(\xi)d\xi}|g\rangle. \tag{142}$$

Here $|g\rangle$ is the initial (ground) state of the system, T is the end of the laser pulse, and t_0 is the initial moment of time.

In this equation, absorption of the XUV photon occurs at the moment t. The propagators from t_0 to t and t to T include the interaction with the strong laser field. Prior to the absorption of the XUV photon the laser field polarizes the electronic wave packet. After the absorption of the XUV photon, the laser field induces the electron oscillations and modifies the electron momentum on the way to the detector.

The eikonal-Volkov approximation can be used between the moments t and T. The action of the operator $e^{-i\int_t^T \hat{H}(\xi)d\xi}$ on the field-free bra $\langle \boldsymbol{q}|$ state is approximated by back-propagating the field-free eikonal state with asymptotic momentum $\boldsymbol{q}$, using the eikonal-Volkov propagator. The specific form appropriate for this problem uses Eq. (96), which includes the adiabatic-type regularization of the amplitude and phase

$$\langle \boldsymbol{q}|e^{-i\int_t^T \hat{H}(\xi)d\xi}|\boldsymbol{r}\rangle \approx \Phi^{*\mathrm{eV}}_{\boldsymbol{q},T}(\boldsymbol{r},t),$$

$$\Phi^{\mathrm{eV}}_{\boldsymbol{q},T}(\boldsymbol{r},t) = P^{\mathrm{ad}}_{\mathrm{WKB}}(\boldsymbol{r},t)\Psi^{V}_{\boldsymbol{q},T}(\boldsymbol{r},t)e^{i\sigma_{\boldsymbol{q},T}(\boldsymbol{r},t)}. \tag{143}$$

To test the accuracy of this approximation, the laser-induced polarization of the electronic wave packet before the moment t can be included exactly, by performing the calculation without the XUV pulse. The comparison of approximate results, which use the eikonal-Volkov propagator for $e^{-i\int_t^T \hat{H}(\xi)d\xi}$, with the exact results obtained by numerical simulations in two fields allows one to directly assess the quality of the eikonal-Volkov approximation. Figure 10, taken from [29], shows such comparison. All results were obtained for the 1D soft-core potential with the ionization potential of Xe, $I_p = 12.13$ eV. The laser wavelength was $\lambda = 800$ nm and the laser field amplitude was $\mathcal{E}_0 = 0.065$ a.u. (intensity $I = 1.5 \times 10^{14}$ W/cm^2). The duration of the XUV pulse was 200 asec, with carrier frequency $\Omega = 3$ a.u. ≈ 81.6 eV and intensity $I_X = 1.0 \times 10^{11}$ W/cm^2.

Figure 10 shows that for the strong field-assisted XUV ionization, the application of the regularized eV function yields excellent quantitative results (5% error). Nonregularized solutions without the amplitude correction increase the error to 50%.

An alternative approach to describe the strong field electron continuum uses the Coulomb-Volkov ansatz [18,19]. Within the framework of the sudden approximation, its limitations were analyzed by Yudin *et al.* [23,83] for sufficiently high frequencies of the XUV photon. In the sudden approximation, the asymptotic momentum of the field-free motion (which determines the coordinate part of the wave function) is time-independent and is given by the energy conservation law for the absorption of one XUV photon. This approximation decouples the effects of the laser field from those of the ionic potential. The validity of this approach depends on the degree of coupling between the laser field and the ionic po-

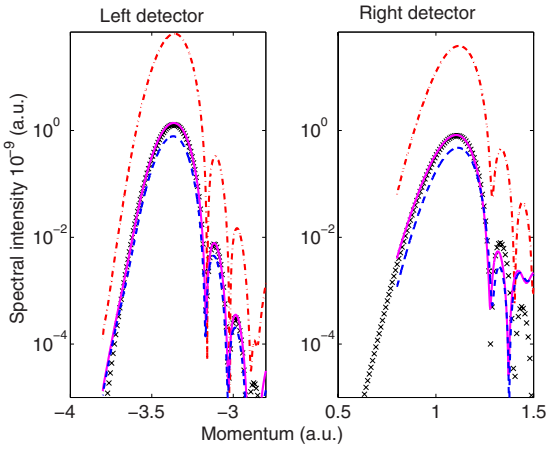

FIG. 10. (Color online) Comparison of different approximations for field-dressed continuum wave functions. Left and right panels show photoelectron spectra on the right and left detectors for the 200 asec XUV pulse arriving at the maximum of the vector potential of the IR field. Numerical results are shown with crosses, results obtained with Volkov functions are shown in red dashed-dotted line, results obtained with nonregularized eV functions are shown as blue dashed line, and results obtained with regularized eV functions with WKB-type amplitude are shown with solid magenta line.

tential. Another limitation of this approach is that it is designed specifically for the purely Coulomb potential of the ion. Although Yudin *et al.* [84] have recently generalized this approach for the H_2^+ ion by using a combination of one-center Coulomb continuum functions, the extension of this approach to complex molecules is not obvious.

We have already stressed that the eikonal-Volkov approach is designed for strong laser fields, since only then the ionic potential might be considered as a perturbation. Additionally, the eikonal-Volkov approach is based on the quasiclassical methods. These methods are justified for strong laser fields, which lead to large action acquired by an electron. However, it is still very useful to check how the eikonal wavefunctions perform in the case of XUV-induced ionization without the presence of the laser field, for sufficiently high photon energies. In this case, the ionization amplitude is determined by the bound-free dipole matrix elements.

Consider atomic hydrogen. We shall compare the length gauge dipole matrix elements for the hydrogen ground state

$$\boldsymbol{d}(\boldsymbol{k}) = \int d\boldsymbol{r}\, \Psi_{\boldsymbol{k}}^{*}(\boldsymbol{r})\boldsymbol{r}\frac{e^{-r}}{\sqrt{\pi}} \tag{144}$$

calculated using different types of continuum states $\Psi_{\boldsymbol{k}}(\boldsymbol{r})$. We shall use (i) plane waves

$$\Psi_{\boldsymbol{k}}(\boldsymbol{r}) = \frac{e^{i\boldsymbol{k}\cdot\boldsymbol{r}}}{(2\pi)^{3/2}}, \tag{145}$$

(ii) the exact continuum wave functions corresponding to the incoming-type solution

$$\Psi_{\boldsymbol{k}}^{(-)}(\boldsymbol{r}) = N_k \frac{e^{i\boldsymbol{k}\cdot\boldsymbol{r}}}{(2\pi)^{3/2}} F(-i\nu, 1, -i(kr + \boldsymbol{k}\cdot\boldsymbol{r})), \tag{146}$$

$$N_k = \sqrt{\frac{2\pi\nu}{1 - e^{-2\pi\nu}}}, \tag{147}$$

where $F(a,b;z)$ is the confluent hypergeometric function, and (iii) the field-free eikonal wave functions corresponding to the incoming-type solution

$$\Psi_{\boldsymbol{k}}^{(-)}(\boldsymbol{r}) = \frac{e^{i\boldsymbol{k}\cdot\boldsymbol{r}}}{(2\pi)^{3/2}} P(\boldsymbol{r}) e^{i\nu\,\ln(kr+\boldsymbol{k}\cdot\boldsymbol{r})}. \tag{148}$$

The continuum states are normalized to momentum. Here the amplitude $P(\boldsymbol{r})$ is given by Eq. (51) with $\boldsymbol{k}_L = \boldsymbol{k}$, $\nu = 1/k$, and

$$\boldsymbol{\nabla} S(\boldsymbol{r},t) = \boldsymbol{k} + \nu\frac{k\boldsymbol{r}/r + \boldsymbol{k}}{(kr + \boldsymbol{k}\cdot\boldsymbol{r})}. \tag{149}$$

In the eikonal approximation the amplitude is

$$P(\boldsymbol{r}) = \left(1 + \frac{1}{k^2 r}\right)^{-1/2}. \tag{150}$$

We choose the quantization axis z along the vector $\boldsymbol{k}$, in this case the only nonzero component of the matrix element is along the quantization axis: $d_z \neq 0$. Let us first compare the exact matrix element

$$|d_z(k)|^2 = \frac{32N_k^2}{\pi^2}\frac{e^{-4\nu\ \mathrm{arccot}\ \nu}}{(1+k^2)^5} \tag{151}$$

with the matrix element calculated using Eq. (148), for the amplitude $P(\boldsymbol{r}) = 1$:

$$|d_z^e(k)|^2 = |d_z(k)|^2 \mathbb{R}_e, \tag{152}$$

$$\mathbb{R}_e = e^{-2\nu\ \arctan\ \nu}\frac{(1+5k^2)^2}{16k^4}. \tag{153}$$

Details of the calculation are given in the Appendix. For $k \to \infty$, the Sommerfeld parameter $\nu = 1/k \to 0$ and $\mathbb{R}_e \to 25/16$. Therefore, when the amplitude correction is ignored $[P(\boldsymbol{r}) = 1]$, the matrix element $|d_z^e(k)|^2$ is asymptotically incorrect.

On the other hand, approximating the amplitude Eq. (150) as

$$P(\boldsymbol{r}) \simeq 1 - \frac{1}{2k^2 r}, \tag{154}$$

we obtain the corresponding matrix element

$$|d_z^{\mathrm{ep}}(k)|^2 = |d_z(k)|^2 \mathbb{R}_{\mathrm{ep}}, \tag{155}$$

$$\mathbb{R}_{\mathrm{ep}} = e^{-2\nu\ \arctan\ \nu}\frac{3 + k^{-2} + 3k^2 + 65k^4 + 64k^6}{64k^4(k^2+1)}. \tag{156}$$

In the limit of large k, $\mathbb{R}_{\mathrm{ep}} \to 1$. Thus the amplitude correction to the eikonal wavefunction is important in ensuring correct asymptotic behavior of the field-free matrix element for $1s$ state of hydrogen.

The plane wave matrix element

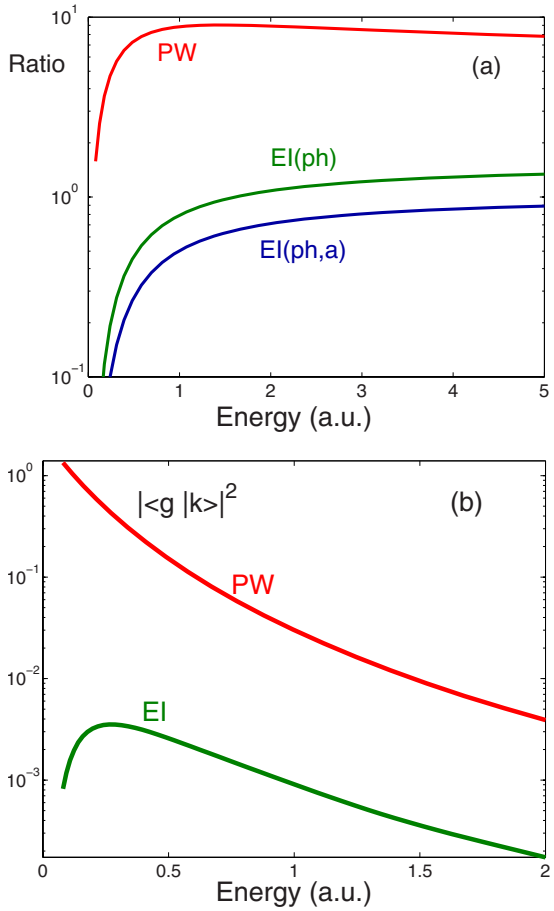

FIG. 11. (Color online) Checking different approximations for bound-free transition matrix elements into the field-free continuum wave functions for hydrogen atom. Panel (a) shows the ratio of various approximate matrix elements to the exact matrix element, as a function of final electron energy. Red solid curve marked as PW shows the ratio $\mathbb{R}_{\rm pw}$ for the plane wave continuum. The ratio $\mathbb{R}_e$ for the eikonal functions with amplitude $P(\boldsymbol{r})=1$ is shown as a solid green curve marked as EI(ph). The ratio $\mathbb{R}_{\rm ep}$ for the eikonal functions with amplitude Eq. (154) is shown as a solid blue curve marked as EI(ph,a). Panel (b) shows orthogonality of the eikonal continuum wave functions [see Eq. (148)] (EI) and the plane waves (PW) to the hydrogen ground state by plotting the overlap $|\int d\boldsymbol{r}\, \Psi^*_{\boldsymbol{k}}(\boldsymbol{r})(e^{-r}/\sqrt{\pi})|^2$.

$$|d_z^{\rm pw}(k)|^2 = \frac{32}{\pi^2}\frac{1}{(1+k^2)^5}\frac{4k^2}{1+k^2} \tag{157}$$

is asymptotically different from the exact solution by a factor of 4. Contrary to the eikonal approximation, the asymptotic value of the matrix element for the plane waves is achieved for extremely high (already relativistic) energies.

Figure 11(a) compares the ratios $\mathbb{R}_e$, $\mathbb{R}_{\rm ep}$, $\mathbb{R}_{\rm pw}=|d_z^{\rm pw}(k)|^2/|d_z(k)|^2$ of various approximate matrix elements to the exact matrix element. Figure 11(b) explores orthogonality of the eikonal continuum wavefunctions in hydrogen to the hydrogen ground state. One can see that the overlap is small even for low-energy states where the eikonal approximation is formally not applicable.

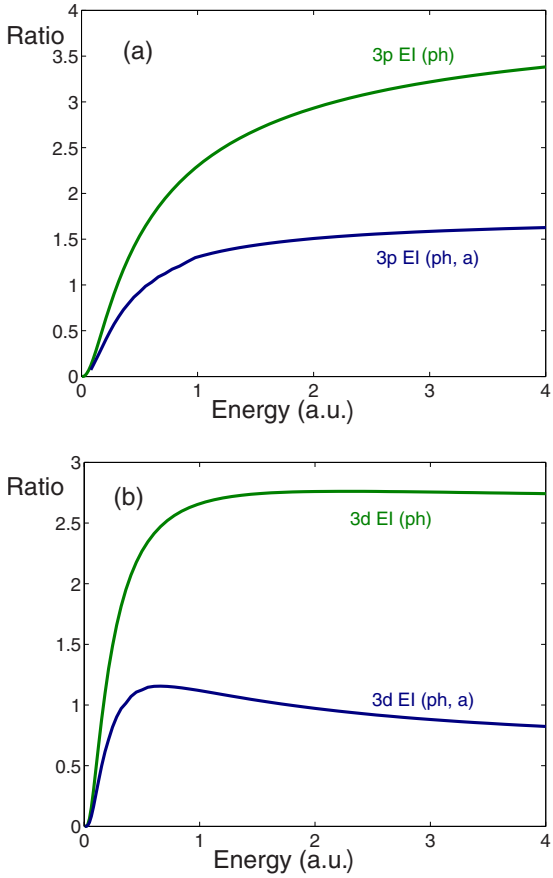

FIG. 12. (Color online) Checking different approximations for bound-free transition matrix elements into the field-free continuum wave functions for hydrogen atom. Panels (a), (b) show the ratio of the approximate matrix element to the exact matrix element for the $3p$ and $3d$ states of the hydrogen atom correspondingly, as a function of the final electron energy. The curves marked as EI(ph) and EI(ph,a) are obtained using the eikonal continuum wave functions without and with the amplitude correction.

Figure 12 shows the ratio of the eikonal and exact the bound-free matrix elements of the z operator for the $3p$ and $3d$ states of the hydrogen atom. In the case of the $3p$ state the continuum s-wave contributes to the transition; the field-free eikonal approximation is most vulnerable in this case. Without the amplitude correction, the agreement is poor. The amplitude correction to the eikonal wavefunction improves the agreement, both for the $3p$ and $3d$ states. As expected, the agreement is worse for the $3p$ state due to the presence of the s wave in the continuum. The eikonal approximation strongly overestimates the contribution of s waves. In these calculations we did not use any regularization procedure, which should improve the agreement for s waves. This issue will be addressed elsewhere.

VII. ANALYTICAL APPROACHES WITHIN THE EVA

It may appear that the eikonal-Volkov functions described in this paper are too complicated for purely analytical treatment. Indeed, SFA in combination with the saddle and stationary point method [39–43] proved to be a very effective

analytical tool of strong field physics. Compared to the SFA, the eikonal-Volkov functions introduce an additional coordinate-dependent phase terms in the S-matrix expressions. These additional phase terms lead to significantly more complex saddle and stationary point equations.

However, this first impression is misleading. The eikonal-Volkov states are in fact well suited for the analytical analysis. In many cases one can adopt an iterative procedure for solving the saddle point equations. This iterative procedure allows one to calculate the S-matrix expressions analytically almost as easily as if using SFA, but still taking into account the effects of the ionic potential.

In the zeroth order, one neglects the potential-dependent phase terms in the eikonal-Volkov functions and solves the saddle point equations given by the SFA. The zeroth order solution yields classical electron trajectories in the laser field, without the ionic potential.

For the next, first-order step, the zero-order solution for the saddle points is inserted into the potential-dependent terms. The resulting equations also yield classical equations of motion, with the ionic potential included perturbatively. They can be solved to obtain the first order solution for the saddle point trajectories.

The key point is that for each energy the zero-order SFA saddle point equations lead to a single or a few trajectories, which then have to be corrected to include the ionic potential. Then, the phase corrections due to the ionic potential have to be calculated not for all integrals and all coordinates, but only for one or two trajectories.

A. Laser-assisted XUV ionization

Let us illustrate the iterative saddle-point procedure for laser-assisted one-photon ionization, triggered by an attosecond XUV pulse. We write the amplitude Eq. (142) as

$$c_X(\boldsymbol{q},t_X) = -i\int_{t_0}^{T} dt \int d\boldsymbol{k}\langle \boldsymbol{q}|\hat{\mathcal{U}}(T,t)|\boldsymbol{k}\rangle \times \langle \boldsymbol{k}|\hat{V}_X(t-t_X)|g\rangle e^{iI_p(t-t_0)}, \tag{158}$$

where $\hat{\mathcal{U}}(T,t)$ is the eikonal-Volkov propagator and $|\boldsymbol{q}\rangle$, $|\boldsymbol{k}\rangle$ are the field-free eikonal states, corresponding to the incoming-type solution

$$\langle \boldsymbol{r}|\boldsymbol{k}\rangle = (2\pi)^{-3/2} e^{i\boldsymbol{k}\cdot\boldsymbol{r}} e^{iG_{0\boldsymbol{k}}^{(-)}(\boldsymbol{r})}, \tag{159}$$

$$\langle \boldsymbol{q}|\boldsymbol{r}\rangle = (2\pi)^{-3/2} e^{-i\boldsymbol{q}\cdot\boldsymbol{r}} e^{-iG_{0\boldsymbol{q}}^{(-)}(\boldsymbol{r})}, \tag{160}$$

where $G_{0\boldsymbol{k}}^{(-)}$ is given by Eq. (21). Compared to Eq. (142), we have neglected the polarization of the ground state by the laser field, introduced the resolution of identity in the basis of the field-free states $\int d\boldsymbol{k}|\boldsymbol{k}\rangle\langle\boldsymbol{k}| + \Sigma|n\rangle\langle n|$, and approximated the continuum states in this decomposition by the field-free eikonal states. By construction, the eikonal-Volkov propagator keeps the continuum states in the continuum. Therefore, we neglect the overlap of back-propagated states $\langle \boldsymbol{q}|\hat{\mathcal{U}}(T,t)$ with the bound states $|n\rangle$ in the resolution of identity, thus arriving at Eq. (158).

Adding the extra integral $\int d\boldsymbol{k}|\boldsymbol{k}\rangle\langle\boldsymbol{k}|$ might look like an unnecessary complication. However, it is extremely useful for the analytical treatment of the problem. Using this device, the interplay between the strong laser field and the ionic potential is transferred completely into the matrix elements of the eikonal-Volkov propagator between the continuum states, $\langle \boldsymbol{q}|\hat{\mathcal{U}}(T,t)|\boldsymbol{k}\rangle$. These matrix elements can be effectively analyzed using the stationary phase method; the same method can be used to deal with the integral over t in Eq. (158). We will show how the interplay between the Coulomb and laser fields hidden in the matrix element $\langle \boldsymbol{q}|\hat{\mathcal{U}}(T,t)|\boldsymbol{k}\rangle$ can be extracted and transferred to the field-free matrix elements $\langle \boldsymbol{k}|\hat{V}_X(t-t_X)|g\rangle$.

In the strong-field approximation (SFA), which neglects the ionic potential, the continuum-continuum matrix element is

$$\langle \boldsymbol{q}|\hat{U}^{(\mathrm{SFA})}(T,t)|\boldsymbol{k}\rangle = \delta[\boldsymbol{q}+\boldsymbol{A}(t)-\boldsymbol{k}] e^{-i(1/2)\int_t^T [\boldsymbol{q}+\boldsymbol{A}(\tau)]^2 d\tau}. \tag{161}$$

Here $\mathbf{A}(t)$ is the vector potential of the IR field. The Coulomb-Volkov sudden ansatz of [23,83,84] makes exactly this approximation for the continuum propagator while using the field-free Coulomb states for the XUV matrix elements, $\langle \boldsymbol{k}|\hat{V}_X(t-t_X)|g\rangle$ in Eq. (158).

When the ionic potential is included together with the laser field, as is done by the eikonal-Volkov propagator, the delta function in the propagator is broadened, its maximum is shifted, and the additional scattering phase is acquired. We will now use the stationary phase method to calculate the integrals in Eq. (158) and evaluate these effects.

We shall use the formalism given by Eq. (158) and additionally insert identity resolved on position states $|\boldsymbol{r}\rangle$

$$c_X(\boldsymbol{q},t_X) = -i\int_{t_0}^{T} dt \int d\boldsymbol{k} \int d\boldsymbol{r}\langle \boldsymbol{q}|\boldsymbol{r}\rangle\langle \boldsymbol{r}|\hat{\mathcal{U}}(T,t)|\boldsymbol{k}\rangle \times \langle \boldsymbol{k}|V_X(t-t_X)|g\rangle e^{iI_p(t-t_0)}. \tag{162}$$

The main time dependence appears in the phase of the eikonal-Volkov propagator. We shall neglect the amplitude correction to the eikonal-Volkov wavefunctions and focus on the phase terms only. Propagating $|\boldsymbol{k}\rangle$ given by Eq. (159) forward from the moment t to the moment T yields

$$\langle \boldsymbol{r}|\hat{\mathcal{U}}(T,t)|\boldsymbol{k}\rangle = \frac{1}{(2\pi)^{3/2}} e^{i[\boldsymbol{k}-\boldsymbol{A}(t)]\cdot\boldsymbol{r}} e^{-i(1/2)\int_t^T d\tau [\boldsymbol{k}-\boldsymbol{A}(t)+\boldsymbol{A}(\tau)]^2} \times e^{-i\int_t^T d\tau\, U[\boldsymbol{r}_L(\tau)]} e^{iG_0^{(-)}[\boldsymbol{r}_L(t)]}. \tag{163}$$

Here the trajectory $\boldsymbol{r}_L(\tau)$ in the IR laser field is specified by its initial (kinetic) momentum $\boldsymbol{k}$ at the instant t and the coordinate $\boldsymbol{r}$ at the instant T

$$\boldsymbol{r}_L(\tau) = \boldsymbol{r} + \int_T^{\tau} dt''[\boldsymbol{k}-\boldsymbol{A}(t)+\boldsymbol{A}(t'')]. \tag{164}$$

According to Eq. (162), the amplitude to find the electron with momentum $\boldsymbol{q}$ can be written via the integrals over the

instant of birth t, the electron momentum at birth $\boldsymbol{k}$, and the final coordinate $\boldsymbol{r}$.

For a short XUV pulse with carrier frequency Ω, the stationary phase point for the instant of birth is t_X—the center of the XUV pulse. The integral over t yields the usual energy conservation law *at the moment of birth* and shows that the peak of the kinetic momentum distribution arises at

$$k^2/2 = \Omega - I_p. \tag{165}$$

This initial kinetic momentum $\boldsymbol{k}$ will be shifted as the electron moves to the detector.

The stationary phase equations for the integral over $\boldsymbol{r}$ [26]

$$\boldsymbol{q} = \boldsymbol{k} - \boldsymbol{A}(t_X) - \Delta\boldsymbol{q}(\boldsymbol{r},\boldsymbol{k}) \tag{166}$$

and for the integral over $\boldsymbol{k}$

$$\boldsymbol{r} = \int_{t_X}^{T} dt''[\boldsymbol{k} - \boldsymbol{A}(t_X) + \boldsymbol{A}(t'')] + (t_X - T)\Delta\boldsymbol{q}(\boldsymbol{r},\boldsymbol{p}) + \boldsymbol{r}_{\text{in}} \tag{167}$$

should be solved to find the momentum $\boldsymbol{k}$ and the coordinate $\boldsymbol{r}$. In both equations we neglected the terms that vanish as $T - t_X \to \infty$. The momentum shift $\Delta\boldsymbol{q}$ in Eqs. (166) and (167) is

$$\Delta\boldsymbol{q}(\boldsymbol{r},\boldsymbol{k}) = \int_{t_X}^{T} d\tau \nabla_{\boldsymbol{r}} U[\boldsymbol{r}_L(\tau)] + \frac{\boldsymbol{k}}{|\boldsymbol{k}|^2} U[\boldsymbol{r}_{\text{in}}]. \tag{168}$$

Here, and in Eq. (167), $\boldsymbol{r}_{\text{in}}$ is the coordinate of birth, which is a function of the dipole matrix element between the ground state and the field-free eikonal state $|\boldsymbol{k}\rangle$ (see [26] for details). In the case of one-photon ionization, the symmetry of the problem dictates that $\boldsymbol{r}_{\text{in}}$ is purely imaginary if the initial state is an eigenstate of the inversion operator [26]. The imaginary part of $\boldsymbol{r}_{\text{in}}$ effectively smooths out the singularity of the potential and plays the role of the impact or soft-core parameter. For estimates one can set $r_{\text{in}} \sim 1/k$. The coordinate of birth acquires a nonzero real part if (i) the initial state is a coherent superposition of eigenstates or (ii) if the field-free Hamiltonian does not commute with the inversion operator.

Now we can solve Eqs. (166) and (167) iteratively. In the zeroth order, we ignore all terms that contain $U(\boldsymbol{r})$ in Eqs. (166) and (167), yielding the SFA result for the stationary points. Indeed, in the zeroth order with respect to $U(\boldsymbol{r})$, the shift Eq. (168) is absent and we obtain the usual SFA result

$$\boldsymbol{q} = \boldsymbol{k} - \boldsymbol{A}(t_X). \tag{169}$$

Note that in the absence of the laser field [i.e., $\boldsymbol{A}(t)=0$] the momentum shift on the way to the detector is equal to zero with or without the potential $U(\boldsymbol{r})$. That is, the slowing down of the field-free electron on the way to the detector is already present in the energy conservation law Eq. (165).

Thus, the SFA result Eq. (169) simply decouples the influence of the laser field and the ionic potential on the electron motion to the detector. The shift $\Delta\boldsymbol{q}$ Eq. (168) naturally characterizes the "Coulomb-laser coupling." Therefore, one can use this shift in the photoelectron spectrum to derive conditions for which electron dynamics in the continuum can be factorized into oscillations in the strong laser field and the acceleration in the ionic potential.

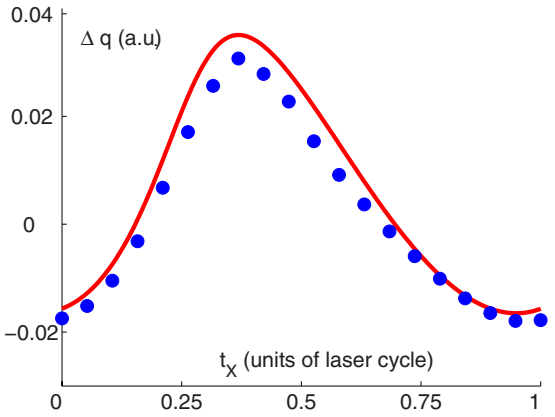

FIG. 13. (Color online) Checking the accuracy of the iterative saddle-point procedure. The momentum shift $\Delta\mathbf{q}$ as a function of the arrival time of the ionizing 200 as XUV pulse. Time is in units of the IR cycle with $\lambda = 800$ nm. Calculations for the soft-core potential Coulomb potential. The solid curve shows analytical results; dots are numerical results.

The zeroth order solution of Eq. (167) is

$$\boldsymbol{r} = \int_{t_X}^{T} dt''[\boldsymbol{k} - \boldsymbol{A}(t_X) + \boldsymbol{A}(t'')] + \boldsymbol{r}_{\text{in}}. \tag{170}$$

Substituting this result into Eq. (164), we obtain the zeroth order stationary electron trajectory

$$\boldsymbol{r}_L^{(0)}(\tau) = \int_{t_X}^{\tau} dt''[\boldsymbol{k} - \boldsymbol{A}(t_X) + \boldsymbol{A}(t'')] + \boldsymbol{r}_{\text{in}}. \tag{171}$$

This trajectory can be substituted into Eq. (166) for $\Delta\boldsymbol{q}$. Thus, the first term in Eq. (168) for $\Delta\boldsymbol{q}$ integrates the attractive force of the ion along the electron trajectory in the laser field given by Eq. (171). The second term in Eq. (168) can be rewritten as a similar integral but along the field-free trajectory

$$\boldsymbol{r}_{\text{FF}}^{(0)}(\tau) = \boldsymbol{r}_{\text{in}} + \boldsymbol{k}(\tau - t_X). \tag{172}$$

Together this treatment yields the following final expression for the momentum shift

$$\Delta\boldsymbol{q} = \int_{t_X}^{T} d\tau \nabla_{\boldsymbol{r}} U[\boldsymbol{r}_L^{(0)}(\tau)] - \int_{t_X}^{T} d\tau \nabla_{\boldsymbol{r}} U[\boldsymbol{r}_{\text{FF}}^{(0)}(\tau)]. \tag{173}$$

Note that the second term in Eq. (173), which appears automatically in the stationary phase analysis, ensures that the momentum shift is equal to zero in the absence of the laser field. As noted above, slowing down of the field-free electron on the way to the detector is already present in the energy conservation law [Eq. (165)].

The accuracy of the stationary-phase analysis is illustrated in Fig. 13, which compares analytical results with the result obtained by evaluating the integrals in Eq. (162) numerically. The potential is $U(x) = -1/\sqrt{x^2 + a^2}$ [56] with $a = 1.59$, yielding $I_p = 12.13$ eV. The IR field is $\mathcal{E}_L(t) = 0.065 \times \cos \omega t$ with a wavelength of 800 nm. The XUV pulse is 200 asec long with

carrier frequency $\Omega=3$ a.u.$=81.6$ eV. Analytical and numerical results agree very well. Soft core potential allows us to set $r_{\text{in}}=0$ for this calculation.

The analytical expression Eq. (173) can be simplified even further. For the Coulomb potential $-Z/r$, the integrals can be estimated analytically

$$|\Delta q| \sim [Z\mathcal{E}_{\text{IR}}(t_X)/k^3]\ln[2k/(|r_{\text{in}}|\omega)], \tag{174}$$

where $|r_{\text{in}}| \propto 1/k$ and $\mathcal{E}_{\text{IR}}$ is the strength of the low-frequency (infrared, IR) laser field.

The corresponding phase shift associated with the Coulomb-laser coupling is $\sim \Delta qR$, where R is the characteristic size of the system. Using Eq. (174), the condition $\Delta qR \ll 1$ yields

$$Z\mathcal{E}_{\text{IR}}R \ll 2^{3/2}(\Omega - I_p)^{3/2}/\ln[4(\Omega - I_p)/\omega]. \tag{175}$$

Setting $\Omega - I_p = 20$ eV and $\mathcal{E}_{\text{IR}}=0.05$ a.u., we see that the scattering phase shift introduced by the Coulomb-laser coupling is small for $R<3$ Å. This is the case for the N_2 molecule, while CO_2 is borderline.

We can now address the interference structures in the high harmonic spectra from molecules. They are related to the shape of the bound electronic orbitals. The XUV absorption process treated above is roughly the time inverse of the XUV emission process responsible for the HHG. Therefore, for $\Delta qR \ll 1$ one can separate the process of XUV emission caused by the electron's recombination with the parent ion from the electron's acceleration by the laser field far from the ion. The main role of the laser field in HHG is to supply the recollision electron with an *asymptotic* momentum $k^2/2 = N\omega - I_p$. Under these conditions, the recombination matrix element from the dressed state can be replaced with a much simpler matrix element between the ground state and the field-free eikonal wave function. Finally, when ΔqR becomes substantial, but still $|\Delta q| \ll |q|$, the Coulomb-laser coupling can be taken into account by substituting $\boldsymbol{k} \to \boldsymbol{k} + \Delta q$ in the field-free recombination matrix elements.

B. High-harmonic generation: Coulomb effects for short trajectories

Although the SFA provides a very important qualitative insight into the nature and the structure of HHG spectra [40], it has two main sources of quantitative inaccuracies. The first deficiency is related to neglecting the electron interaction with the core. The second deficiency arises due to neglect of such effects as polarization of the ionic core and multielectron effects (see, e.g., [76,75]). Here we shall focus on inaccuracies related to the Coulomb effects in the electron continuum.

As shown above, in the eikonal approximation, the saddle point equations for the integral expressions for quantum amplitudes are nothing but the classical equations of motion, with the ionic potential included perturbatively.

This observation provides a simple framework for improving the quantitative accuracy of HHG description based on the factorized form of the HHG amplitude [41]. In this form, the emission amplitude is written as a product of the amplitudes of ionization, propagation and recombination. The amplitudes are calculated for a specific trajectory (or a few trajectories) that realizes the saddle point of the multidimensional integral [40]. Individual consequences of neglecting the ionic potential can be gradually fixed by using the classical analysis.

Let us look at one of the improvements. Neglecting the ionic potential in the electron trajectories leads to an overestimate of the excursion times. Let us fix the time of the electron return to the core, t_R. This time corresponds to a specific moment of ionization t_B. To arrive at the core at the same moment of time, the electron that feels the long-range attractive potential of the ion would have to be "born" at earlier times, $t_B - \Delta t_B$, compared to the case when the long-range attraction is neglected. The shift Δt_B may have significant implications.

The state of the art approach to calculating ionization rates in multielectron systems [85–87] in strong low-frequency fields $\mathcal{E}_0 \cos \omega t$ relies on the quasistatic approximation: The time-dependent ionization rate $\Gamma(t)$ is calculated for each phase of birth ωt_B using a static field with strength $\mathcal{E}=\mathcal{E}_0 \cos \omega t_B$. The exponential dependence of the tunneling rate on the strength of the electric field $\propto \exp[-2(2I_p)^{3/2}/(3\mathcal{E}_0 \cos \omega t_B)]$ means that even small changes in the moment of ionization and hence in $\cos \omega t_B$ may lead to significant changes in the ionization probability. In the quasistatic approximation this issue becomes critical for the phases of birth near the zero of the electric field $\omega t_B \sim \pi/2$, i.e., for the so-called "short" trajectories. Since at earlier times the laser field is stronger, neglecting the shift Δt_B in $\cos(\omega t_B - \Delta \omega t_B)$ results in an exponential suppression of harmonics originating from the "shortest" trajectories.

Figure 14(a) shows the effect of Δt_B in the quasistatic approximation, plotting the ionization amplitude as a function of the moment of return t_R. The dashed (blue) curve shows the tunnel ionization amplitude $a_T(t_B(t_R))$ for the moments of birth calculated without treating the Coulomb effects in the continuum. The solid (red) curve plots the same tunneling amplitude, but for the moments of birth shifted due to the Coulomb effects. In the quasistatic approximation, the effect of the shift Δt_B on the ionization amplitude is dramatic. To calculate the quasistatic ionization amplitude, we used the static PPT formula [28], setting the laser parameters to $I=2\times 10^{14}$ W/cm^2, $\lambda=800$ nm, the ionization potential to $I_p=15.5$ eV, and the angular momentum quantum number $l=0$. To find the connection between the moment t_B and the moment t_R of return to the initial position, we have propagated the classical trajectory (with or without the Coulomb potential), starting with zero initial velocity at the "exit" of the tunnel z_B given by the strong field approximation.

To find z_B for an arbitrary phase of birth, we adapted the imaginary time method developed by Popov and co-workers [27,28,31,32] for tunneling in low-frequency fields. For arbitrary Keldysh parameter γ it yields

$$z_B(t_B) = \frac{\mathcal{E}_0}{\omega^2}[\cos(\omega t_B) - \cos(\phi_0) + S\omega(t_B - t_0)], \tag{176}$$

$$\phi_0 = \arcsin(\sqrt{P}) + i\,\text{arccosh}(S/\sqrt{P}), \tag{177}$$

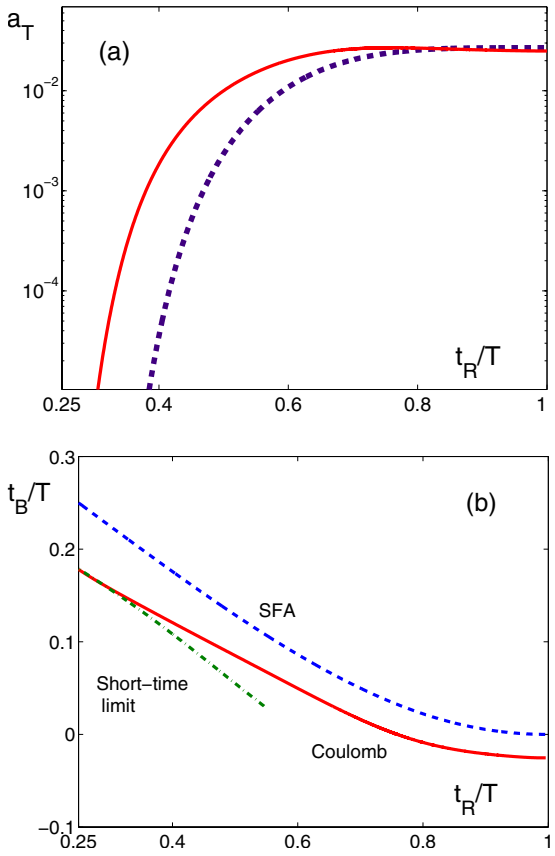

FIG. 14. (Color online) (a) Ionization amplitude as a function of the moment of return t_R; t_R is in the units of laser cycle. The dashed (blue) curve shows tunnel ionization amplitude $a_T[t_B(t_R)]$ for the moments of birth calculated neglecting the Coulomb effects in the continuum. The solid (red) curve shows the same tunneling amplitude, but for the moment of birth shifted due to the Coulomb effects. (b) t_B vs t_R with (solid red curve marked as "Coulomb") and without (dashed blue curve marked as "SFA") the Coulomb potential taken into account. Dashed-dotted (green) line shows "short-time" analytical approximation to the solid curve. In this calculation $I=2\times10^{14}$ W/cm^2, $\lambda=800$ nm, and $I_p=15.5$ eV.

$$P=\frac{1}{2}(1+\gamma^2+S^2-\sqrt{D}), \tag{178}$$

$$D=(1+\gamma^2)^2+S^4+2S^2(\gamma^2-1), \tag{179}$$

$$S=\sin(\omega t_B). \tag{180}$$

Here $\phi_0=\omega t_0$ indicates the start of the electron underbarrier motion. In a static field $z_B(t_B)$ is real, while in the oscillating field it becomes complex. The coordinate of the exit from the tunnel is given by the real part of Eq. (176). Details of the derivation will be given elsewhere [88].

The calculated dependence $t_B=t_B(t_R)$ with and without the Coulomb potential is shown in Fig. 14(b). Since the change in the quasistatic ionization rates is largest for the shortest trajectories, we have also derived an analytical expression for the connection between t_B and t_R in this limit

$$\omega t_R=\frac{3\pi}{2}-2\omega t_B-\frac{3}{\mathcal{E}_0 z_B(t_B)^2}. \tag{181}$$

The first two terms on the right hand side are the SFA result, while the third reflects the effect of the Coulomb potential. This result is shown in Fig. 14(b) (dashed-dotted line), and the agreement with the numerical calculation is good for short times.

The derivation of Eq. (181) uses the classical equations of motion suggested by the eikonal approximation, i.e., it includes the ionic potential perturbatively. The requirement that the electron returns to its initial position means that the total displacement between t_B and t_R is equal to zero

$$0=\int_{t_B}^{t_R} v_z(t)dt. \tag{182}$$

In a linearly polarized field, the trajectory is along the z axis, and the velocity $v_z(t)$ includes electron oscillations in the laser field $k_L(t)$ as well as the contributions due to the Coulomb potential. In the eikonal approximation,

$$v_z(t)=k_L(t)dt+\int_{t_B}^{t} dt' F_C(z_L(t')), \tag{183}$$

where F_C is the attractive Coulomb force and $z_L(t)$ is the electron trajectory in the laser field. To be specific, let us assume that at the moment t_B the laser electric field is positive, the electron is "born" at negative coordinate $-z_B$. The Coulomb force is positive

$$F_C(z_L(t))=\frac{1}{z_L(t)^2}. \tag{184}$$

For very short trajectories, the electron displacement from the position of birth is small compared to z_B, and we can approximate the Coulomb force as

$$F_C(z_L(t))\approx\frac{1}{z_B(t_B)^2}. \tag{185}$$

With this approximation, the solution of Eq. (182) becomes straightforward and leads to the result Eq. (181).

The quasistatic approximation strongly underestimates the ionization probability near the zeros of the laser field. It neglects the role of nonadiabatic tunneling [66], which is important not only for moderate values of $\gamma\sim1$, but also for small γ near the zeroes of the instantaneous electric field. Correspondingly, the effect of the Coulomb potential-induced shift of $t_B=t_B(t_R)$ is overestimated when using the quasistatic approximation for calculating the tunneling rates.

Figure 15 shows the dependence of the ionization amplitude $a_T(t_B(t_R))$ on t_R, calculated using expressions of Ref. [66] with and without the time shift Δt_B due to the Coulomb potential. The laser parameters and the ionization potential are the same as in Fig. 14. The dashed (blue) curve shows the calculation which neglects the Coulomb potential in the relation $t_B(t_R)$. As expected, the nonadiabatic tunneling increases the ionization amplitude for the shortest trajectories

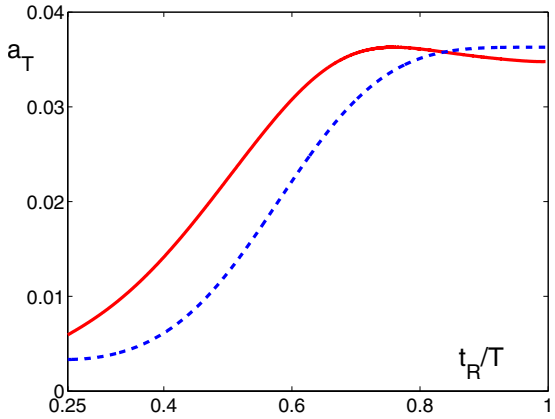

FIG. 15. (Color online) Nonadiabatic ionization amplitude a_T as a function of the moment of return t_R, where t_R is in the units of laser cycle. The dashed (blue) curve shows tunnel ionization amplitude $a_T(t_B(t_R))$ for moments of birth calculated neglecting Coulomb effects in the continuum. The solid (red) curve shows the same tunneling amplitude, but for the moment of birth shifted due to the Coulomb effects. As in Fig. 14, $I=2\times10^{14}$ W/cm^2, $\lambda=800$ nm, and $I_p=15.5$ eV.

significantly compared to the quasistatic approximation [see Fig. 14(a)]. The Coulomb corrections to t_B increase the ionization amplitude, see solid (red) curve.

VIII. CONCLUSIONS

We have used the eikonal approximation to incorporate the effects of the binding potential on the continuum motion of one and two electrons strongly driven by the laser field. We have derived both the phase and amplitude corrections to the Volkov wavefunctions, and analyzed several additional approximations to both terms.

We have shown that, in the long-time limit, the eikonal Volkov states take the form of quasienergy states for the strongly driven continuum electron. We developed the EVA, which is meant to substitute the SFA for all strong-field problems.

The EVA is equally justified for both (i) "horizontal" strong-field ionization, which liberates the electron with near zero velocity but away from the core, and also (ii) for the "vertical" one-photon ionization triggered by an XUV photon, which liberates the electron near the core but with high excess energy.

The particular details of one photon ionization, as opposed to the strong-field ionization, emphasize the importance of the time-dependent WKB-type amplitude correction to the wave function and the regularization procedure. At the same time, the regularization procedure and the amplitude correction are not needed for the case of strong field ionization since (i) the electron is born away from the core with small velocity, and (ii) the regularization procedure relies on additional adiabatic approximation, which is not justified for strong-field ionization.

Further, the eikonal-Volkov states have been generalized to treat the hard collisions between the electron and the ion, thus enabling applications of the eikonal approximation to the complete range of strong-field processes. It completes the foundation of the EVA approach. The EVA approach involves the S-matrix-based expressions which partition the interaction potential into a short-range singular part and a long-range nonsingular part. The eikonal-Volkov states are build to describe the electron motion in the long-range part of the potential, while hard collision is included in a Born-like series with respect to the short-range singular part of the potential.

We have also developed an iterative analytical procedure to solve multiple integrals arising in the S-matrix expressions within the EVA. The procedure relies on the saddle-point method, where the saddle-point equations are solved iteratively with respect to the terms containing the binding potential.

The time-dependent phase associated with the initial distortion of the field-free continuum $G_{0\boldsymbol{k}}(\boldsymbol{r}_0)$ is important for strong-field ionization, since for the electrons with small drift momentum the initial distortion takes a long time to propagate away from the interaction region. The phase $G_{0\boldsymbol{k}}(\boldsymbol{r}_0)$ is also crucial in the analytical treatment, when one inserts identity, resolved on the basis of the field-free eikonal states. This approach is very convenient, e.g., for one-photon ionization in the presence of a strong laser field.

The key aspect of strong-field scattering is that in general Born-like series in the number of hard collisions converge rapidly (while the number of soft collisions, well described in the eikonal approximation, can be large). We expect that narrow resonances in the continuum, ubiquitous in the field-free scattering problems, will not survive in the presence of intense fields. While it remains to be demonstrated, we expect that eikonal-Volkov states augmented by single hard collision will be adequate to describe the main features of scattering in the strong laser field.

ACKNOWLEDGMENTS

We are indebted to S. Patchkovskii for reading the manuscript and making many valuable comments and suggestions. We acknowledge stimulating discussions with V. Averbukh, S. Patchkovskii, M. Frolov, C. Chirila, W. Becker, N. Manakov, S. Goreslavski, and G. Yudin. M.I., M.S., and O.S. acknowledge financial support by the NSERC SRO. M.I. also acknowledges support from the Alexander von Humboldt Foundation.

APPENDIX

The exact matrix element for bound-continuum transition for hydrogen and hydrogen-type ions can be calculated analytically using the etalon integral (see [89,84])

$$J(\lambda,\nu)=\int\frac{d\boldsymbol{r}}{r}e^{-\lambda r}e^{i(\boldsymbol{q}-\boldsymbol{k})\boldsymbol{r}}F(i\nu;1;i(kr+\boldsymbol{k}\cdot\mathbf{r}))$$
$$=\frac{4\pi}{\lambda^2+(\boldsymbol{q}-\boldsymbol{k})^2}\left[\frac{q^2+(\lambda-ik)^2}{\lambda^2+(\boldsymbol{q}-\boldsymbol{k})^2}\right]^{-i\nu}. \quad \text{(A1)}$$

Analogously, we introduce the etalon integral to calculate the

bound-continuum matrix elements for the eikonal continuum states

$$J^{\mathrm{EI}}(\lambda,\nu) = \int \frac{d\boldsymbol{r}}{r} e^{-\lambda r} e^{i(\boldsymbol{q}-\boldsymbol{k})\boldsymbol{r}} e^{-i\nu \ln(kr+\boldsymbol{k}\cdot\boldsymbol{r})} = \frac{4\pi\Gamma(1+i\nu)}{\lambda^2+(\boldsymbol{q}-\boldsymbol{k})^2}\left[\frac{2k}{\lambda - i(\boldsymbol{q}-\boldsymbol{k})^2}\right]^{-i\nu}. \quad \text{(A2)}$$

Thus, for the $1s$ state of hydrogen the matrix element Eq. (144) with the exact continuum function Eq. (146) yields

$$d_z(k) = 2\sqrt{2} i\pi \frac{\partial^2}{\partial\lambda\partial q_z} J(\lambda,\nu)\big|_{\boldsymbol{q}=0,\lambda=1}. \quad \text{(A3)}$$

Analogously, using the etalon integral Eq. (A2) for the eikonal continuum state Eq. (148) and $P(\boldsymbol{r})=1$ we obtain

$$d_z^e(k) = 2\sqrt{2} i\pi \frac{\partial^2}{\partial\lambda\partial q_z} J^{\mathrm{EI}}(\lambda,\nu)\big|_{\boldsymbol{q}=0,\lambda=1}. \quad \text{(A4)}$$

Finally, for the eikonal continuum state and the amplitude $P(\boldsymbol{r})$ in the form given by Eq. (154) using Eq. (A2) we obtain

$$d_z^{\mathrm{ep}}(k) = 2\sqrt{2} i\pi \left[\left(\frac{\partial^2}{\partial\lambda\partial q_z} + \frac{1}{2k^2}\frac{\partial}{\partial q_z}\right) J^{\mathrm{EI}}(\lambda,\nu)\right]_{\boldsymbol{q}=0,\lambda=1}. \quad \text{(A5)}$$

[1] U. Mohideen, M. H. Sher, H. W. K. Tom, G. D. Aumiller, O. R. Wood, R. R. Freeman, J. Bokor, and P. H. Bucksbaum, Phys. Rev. Lett. **71**, 509 (1993).
[2] B. Yang, K. J. Schafer, B. Walker, K. C. Kulander, P. Agostini, and L. F. DiMauro, Phys. Rev. Lett. **71**, 3770 (1993).
[3] P. Agostini and L. F. DiMauro, Rep. Prog. Phys. **67**, 813 (2004).
[4] B. Walker, B. Sheehy, L. F. DiMauro, P. Agostini, K. J. Schafer, and K. C. Kulander, Phys. Rev. Lett. **73**, 1227 (1994).
[5] M. Lein, J. P. Marangos, and P. L. Knight, Phys. Rev. A **66**, 051404(R) (2002).
[6] T. Zuo, A. D. Bandrauk, and P. B. Corkum, Chem. Phys. Lett. **259**, 313 (1996).
[7] M. Lein, N. Hay, R. Velotta, J. P. Marangos, and P. L. Knight, Phys. Rev. Lett. **88**, 183903 (2002).
[8] M. Spanner, O. Smirnova, P. Corkum, and M. Ivanov, J. Phys. B **37**, L243 (2004).
[9] S. N. Yurchenko, S. Patchkovskii, I. V. Litvinyuk, P. B. Corkum, and G. L. Yudin, Phys. Rev. Lett. **93**, 223003 (2004).
[10] J. Itatani, J. Levesque, D. Zeidler, H. Niikura, H. Pepin, J. C. Kieffer, P. B. Corkum, and D. M. Villeneuve, Nature (London) **432**, 867 (2004).
[11] T. Kanai, S. Minemoto, and H. Sakai, Nature (London) **435**, 470 (2005).
[12] M. Weckenbrock, A. Becker, A. Staudte, S. Kammer, M. Smolarski, V. R. Bhardwaj, D. M. Rayner, D. M. Villeneuve, P. B. Corkum, and R. Dörner, Phys. Rev. Lett. **91**, 123004 (2003).
[13] L. V. Keldysh, Zh. Eksp. Teor. Fiz. **47**, 1945 (1964) [Sov. Phys. JETP **20**, 1307 (1965)].
[14] H. R. Reiss, Phys. Rev. A **22**, 1786 (1980); **42**, 1476 (1990); Prog. Quantum Electron. **16**, 1 (1992).
[15] F. H. M. Faisal, J. Phys. B **6**, L89 (1973).
[16] D. M. Wolkow, Z. Phys. **94**, 250 (1935).
[17] O. Smirnova, M. Spanner, and M. Ivanov, J. Phys. B **39**, S307 (2006).
[18] M. Jain and N. Tzoar, Phys. Rev. A **18**, 538 (1978).
[19] P. Cavalieri, G. Ferrante, and C. Leone, J. Phys. B **13**, 4495 (1980).
[20] J. Z. Kaminski, Phys. Scr. **34**, 770 (1986); Phys. Rev. A **37**, 622 (1988).
[21] J. Z. Kaminski, A. Jaron, and F. Ehlotzky, Phys. Rev. A **53**, 1756 (1996).
[22] J. Z. Kaminski and F. Ehlotzky, Phys. Rev. A **54**, 3678 (1996).
[23] G. L. Yudin, S. Patchkovskii, P. B. Corkum, and A. D. Bandrauk, J. Phys. B **40**, F93 (2007).
[24] G. L. Yudin, S. Chelkowski, and A. D. Bandrauk, J. Phys. B **39**, L17 (2006).
[25] M. F. Ciappina, C. C. Chirila, and M. Lein, Phys. Rev. A **75**, 043405 (2007).
[26] O. Smirnova, A. S. Mouritzen, S. Patchkovskii, and M. Yu. Ivanov, J. Phys. B **40**, F197 (2007).
[27] A. M. Perelomov and V. S. Popov, Zh. Eksp. Teor. Fiz. **52**, 514 (1967) [Sov. Phys. JETP **25**, 336 (1967)].
[28] A. M. Perelomov, V. S. Popov, and M. V. Terent'ev, Zh. Eksp. Teor. Fiz. **50**, 1393 (1966) [Sov. Phys. JETP **23**, 924 (1966)].
[29] O. Smirnova, M. Spanner, and M. Yu. Ivanov, J. Phys. B **39**, S323 (2006).
[30] R. J. Glauber, in *High-Energy Collision Theory*, edited by A. O. Barut and W. E. Brittin, Lectures in Theoretical Physics Vol. 1 (Interscience, New York, 1959).
[31] A. M. Perelomov, V. S. Popov, and M. V. Terent'ev, Zh. Eksp. Teor. Fiz. **51**, 309 (1966) [Sov. Phys. JETP **24**, 207 (1967)].
[32] V. S. Popov, V. P. Kuznetsov, and A. M. Perelomov, Zh. Eksp. Teor. Fiz. **53**, 331 (1967) [Sov. Phys. JETP **26**, 222 (1968)].
[33] Joel I. Gersten and Marvin H. Mittleman, Phys. Rev. A **12**, 1840 (1975).
[34] H. K. Avetissian, A. G. Markossian, G. F. Mkrtchian, and S. V. Movsissian, Phys. Rev. A **56**, 4905 (1997).
[35] S. Gordienko and J. Meyer-ter-Vehn, in *Laser Interaction with Matter*, edited by O. N. Krokhin, S. Y. Gus'kov, and Yu. A. Merkul'ev, Proc. SPIE Vol. 5228 (SPIE, Bellingham, WA, 2003), p. 416.
[36] F. H. M. Faisal and G. Schlegel, J. Phys. B **38**, L223 (2005); J. Mod. Opt. **53**, 207 (2006).
[37] C. C. Chirila and R. M. Potvliege, Phys. Rev. A **71**, 021402(R) (2005).
[38] A. Becker and F. Faisal, J. Phys. B **38**, R1 (2005).
[39] W. Becker, A. Lohr, and M. Kleber, Quantum Semiclassic. Opt. **7**, 423 (1995); R. Kopold, W. Becker, and M. Kleber, Opt. Commun. **179**, 3950 (2000).
[40] M. Lewenstein, P. Balcou, M. Y. Ivanov, A. L'Huillier, and P. B. Corkum, Phys. Rev. A **49**, 2117 (1994).

[41] M. Yu. Ivanov, T. Brabec, and N. Burnett, Phys. Rev. A **54**, 742 (1996).
[42] W. Becker, A. Lohr, and M. Kleber, Quantum Semiclassic. Opt. **7**, 423 (1995) R. Kopold, W. Becker, and M. Kleber, Opt. Commun. **179**, 3950 (2000).
[43] D. B. Milosevic and W. Becker, Phys. Rev. A **66**, 063417 (2002).
[44] M. V. Frolov, N. L. Manakov, E. A. Pronin, and A. F. Starace, Phys. Rev. Lett. **91**, 053003 (2003).
[45] N. L. Manakov, A. F. Starace, A. V. Flegel, and M. V. Frolov, Zh. Eksp. Teor. Fiz. **76**, 316 (2002) [JETP Lett. **76**, 258 (2002)].
[46] C. Figueira de Morisson Faria, H. Schomerus, and W. Becker, Phys. Rev. A **66**, 043413 (2002).
[47] U. Fano and J. W. Cooper, Rev. Mod. Phys. **40**, 441 (1968).
[48] J. Wassaf, V. Veniard, R. Taieb, and A. Maquet, Phys. Rev. Lett. **90**, 013003 (2003).
[49] S. V. Popruzhenko, Ph. A. Korneev, S. P. Goreslavski, and W. Becker, Phys. Rev. Lett. **89**, 023001 (2002).
[50] K. Krajewska, Ilya I. Fabrikant, and A. F. Starace, Phys. Rev. A **74**, 053407 (2006); B. Borca, M. V. Frolov, N. L. Manakov, and A. F. Starace, Phys. Rev. Lett. **88**, 193001 (2002).
[51] W. Henneberger, Phys. Rev. Lett. **21**, 838 (1968).
[52] Stanley J. Farlow, *Partial Differential Equations for Scientists and Engineers*, 1st ed. (Dover, New York, 1993).
[53] L. D. Landau and E. M. Lifshitz, *Quantum Mechanics: Non-Relativistic Theory*, 3rd ed. (Butterworth-Heinemann, London, 1981).
[54] This assumption does not limit the generality of Eq. (24). If $|k_x|>|k_y|$, $|k_z|$, then $z\rightarrow x$, $z'\rightarrow x'$, $k_x\rightarrow k_z$.
[55] L. Rosenberg, Phys. Rev. D **8**, 1833 (1973).
[56] J. Javanainen, J. H. Eberly, and Q. Su, Phys. Rev. A **38**, 3430 (1988).
[57] The WKB amplitude for 1D autonomous system has the form $P^{\mathrm{WKB}}(x)=\sqrt{|k/[\partial S(x)/\partial x]|}$, where k is asymptotic momentum, and $\partial S/\partial x=k(x)=\sqrt{k^2-2U(\boldsymbol{r})}$. In Eq. (51) we have introduced an "adiabatic WKB" amplitude in analogy with the structure of $P^{\mathrm{WKB}}(x)$ and assuming slow time dependence.
[58] V. P. Maslov and M. V. Fedoriuk, *Semi-Classical Approximation in Quantum Mechanics* (Springer, New York, 2001).
[59] Yu. A. Kravtsov and Yu. I. Orlov, *Caustics, Catastrophes and Wave Fields* (Springer, New York, 1993, 1999).
[60] H. Shirley, Phys. Rev. **138**, B979 (1965).
[61] V. I. Ritus, Zh. Eksp. Teor. Fiz. **51**, 1544 (1966).
[62] Ya. B. Zeldovich, Zh. Eksp. Teor. Fiz. **51**, 1492 (1966).
[63] H. Sambe, Phys. Rev. A **7**, 2203 (1973).
[64] W. H. Adams, J. Chem. Phys. **45**, 3422 (1966).
[65] C. J. Joachain, *Quantum Collision Theory* (North-Holland, Amsterdam, 1983).
[66] G. L. Yudin and M. Yu. Ivanov, Phys. Rev. A **64**, 013409 (2001).
[67] M. Uiberacker *et al.*, Nature (London) **446**, 627 (2007).
[68] P. B. Corkum, Phys. Rev. Lett. **71**, 1994 (1993).
[69] D. B. Milosevic, G. G. Paulus, D. Bauer, and W. Becker, J. Phys. B **39**, R203 (2006).
[70] O. Smirnova, M. Spanner, and M. Ivanov, J. Mod. Opt. **54**, 1019 (2007).
[71] R. T. Sharp and G. K. Horton, Phys. Rev. **90**, 317 (1953).
[72] James D. Talman and William F. Shadwick, Phys. Rev. A **14**, 36 (1976).
[73] Qin Wu and Weitao Yang, J. Chem. Phys. **118**, 2498 (2003).
[74] Miguel A. L. Marques, Carsten A. Ullrich, Fernando Nogueira, Angel Rubio, Kieron Burke, and Eberhard K. U. Gross, *Time-Dependent Density Functional Theory*, Lecture Notes in Physics (Springer-Verlag, Berlin, Heidelberg, 2006).
[75] S. Patchkovskii, Z. Zhao, T. Brabec, and D. M. Villeneuve, Phys. Rev. Lett. **97**, 123003 (2006); J. Chem. Phys. **126**, 114306 (2007).
[76] R. Santra and A. Gordon, Phys. Rev. Lett. **96**, 073906 (2006).
[77] P. P. Ewald, Ann. Phys. **64**, 253 (1921).
[78] A. M. Lee, S. W. Taylor, J. P. Dombroski, and P. M. W. Gill, Phys. Rev. A **55**, 3233 (1997).
[79] See, e.g., D. Cook, *Handbook of Computational Quantum Chemistry* (Dover Publications, New York, 2005).
[80] C. Figueira de Morisson Faria, X. Liu, W. Becker, and H. Schomerus, Phys. Rev. A **69**, 021402(R) (2004).
[81] J. Itatani, F. Quere, G. L. Yudin, M. Y. Ivanov, F. Krausz, and P. B. Corkum, Phys. Rev. Lett. **88**, 173903 (2002).
[82] E. Goulielmakis *et al.*, Science **305**, 1267 (2004); **317**, 769 (2007).
[83] A. M. Dykhne and G. L. Yudin, Usp. Fiz. Nauk **121**, 157 (1977) [Sov. Phys. Usp. **20**, 80 (1977)].
[84] G. L. Yudin, S. Chelkowski, and A. D. Bandrauk, J. Phys. B **39**, L17 (2006).
[85] A. Scrinzi, Phys. Rev. A **61**, 041402(R) (2000).
[86] M. B. Gaarde, M. Murakami, and R. Kienberger, Phys. Rev. A **74**, 053401 (2006).
[87] R. Santra, R. W. Dunford, and L. Young, Phys. Rev. A **74**, 043403 (2006).
[88] O. Smirnova and M. Ivanov (to be published).
[89] A. Nordsieck, Phys. Rev. **93**, 785 (1954).